An intercomparison of satellite, airborne, and ground-level observations with WRF-CAMx simulations of NO_2 columns over Houston, TX during the September 2021 TRACER-AQ campaign

M. Omar Nawaz[1], Jeremiah Johnson[2], Greg Yarwood[2], Benjamin de Foy[3], Laura Judd[4], and Daniel L. Goldberg[1]

[1]Department of Environmental and Occupational Health, George Washington University, Washington, DC, 20052, USA

[2]Ramboll, Novato, California, 94945, USA

[3]Saint Louis University, St. Louis, Missouri, 63103, USA

[4]NASA Langley, Hampton, Virginia, 23666, USA

Correspondence to M. Omar Nawaz (nawaz.muhammad@email.gwu.edu)

Abstract. Nitrogen dioxide (NO_2) is a precursor of ozone (O_3) and fine particulate matter ($PM_{2.5}$) – two pollutants that are above regulatory guidelines in many cities. Bringing urban areas into compliance of these regulatory standards motivates an understanding of the distribution and sources of NO_2 through observations and simulations. The TRACER-AQ campaign, conducted in Houston, TX in September 2021, provided a unique opportunity to compare observed NO_2 columns from ground-, airborne-, and satellite-based spectrometers. In this study, we investigate how these observational datasets compare, and simulate column NO_2 using WRF-CAMx with fine resolution (444 x 444 m^2) comparable to the airborne column measurements. We compare WRF-simulated meteorology to ground-level monitors and find good agreement. We find that observations from the GEOstationary Coastal and Air Pollution Events (GEO-CAPE) Airborne Simulator (GCAS) instrument were strongly correlated (r^2=0.79) to observations from Pandora spectrometers with a slight high bias (NMB=3.4%). Remote-sensing observations from the TROPOspheric Monitoring Instrument (TROPOMI) were generally well correlated with Pandora observations (r^2=0.73) with a negative bias (NMB=-22.8%). We intercompare different versions of TROPOMI data and find similar correlations across three versions but slightly different biases (from -22.8% in v2.4.0 to -18.2% in the NASA MINDS product). Compared to Pandora observations, the WRF-CAMx simulation had reduced correlation (r^2=0.34) and a low bias (-21.2%) over the entire study region. We find particularly poor agreement between simulated NO_2 columns and GCAS-observed NO_2 columns in downtown Houston an area of high population and roadway densities. These findings point to a potential underestimate of NOx emissions (NO_X = NO + NO_2) from sources associated with the urban core of Houston, such as mobile sources, in the WRF-CAMx simulation driven by the Texas state inventory; and further investigation is recommended.

Deleted:
Deleted: GEOCAPE Airborne Simulator (GCAS)
Deleted: 80
Deleted: negligible
Deleted: 0.1
Deleted: instrument
Deleted: 4
Deleted: 5
Deleted: 5
Deleted: vehicle
Deleted: Houston's
Deleted: ¶

1 Introduction

Nitrogen dioxide (NO_2) is a critical precursor to criteria air pollutants (i.e., ozone or "O_3" and fine particulate matter or "$PM_{2.5}$") that are above regulatory thresholds in many urban areas. Exposure to NO_2 is also directly associated with asthma exacerbation in vulnerable groups (Achakulwisut et al., 2019; Anenberg et al., 2022) and premature death (Huang et al., 2021). Due to its short atmospheric lifetime (de Foy et al., 2014), observations of NO_2 can reveal fine-scale patterns associated with sources. A major source of NO_2 is fossil-fuel combustion (McDuffie et al., 2020) and in many urban airsheds this is the dominant contributor to NO_2; however, other natural sources – like lightning (Murray, 2016) and soil microbes (Hudman et al., 2012) – along with fires (Jin et al., 2021) and tropospheric-stratospheric NO_2 exchange also contribute to tropospheric NO_2 levels. The health burden, sources, and short atmospheric lifetime of NO_2 all compound in urban environments where there are large populations, diverse contributors, and unique fine-scale patterns in NO_2 levels.

In the US city of Houston, Texas – the fifth most populous metropolitan region in the US (United States Census Bureau, 2022) – NO_2 is a major concern (Mazzuca et al., 2016) due to its role as a precursor of the formation of O_3 and $PM_{2.5}$. While NO_2 itself nor $PM_{2.5}$ exceed their respective US EPA National Ambient Air Quality Standards (NAAQS), Houston is in moderate nonattainment of the 8-hour Ozone (2015) NAAQS. The large petrochemical industry in Houston emits NO_2 in addition to other common heavy emitting sources associated with coastal urban environments like vehicles, power stations, and shipping channels (Kim et al., 2011). The co-location of this large population with high levels of NO_2 presents a major public health concern that motivates research to better understand the sources that are most culpable in contributing to air pollution. Major highways like the I-610 interstate, the I-10 interstate, and Beltway 8 have heavy vehicle traffic that are responsible for elevated NO_2 concentrations (Miller et al., 2020). Large power stations and industrial facilities operate within and around the Houston metropolitan area and these point sources – along with a large shipping channel – are responsible for NO_2 plumes (Luke et al., 2010). Characterizing the unique imprints of these disparate sources remains a question of scientific concern. There is also evidence that low-income and non-white populations in Houston are disproportionally affected by air pollutants such as NO_2 (Demetillo et al., 2020).

Synchronous observations of NO_2 column densities from aircraft, ground-based, and satellite spectrometers coincided in September 2021 during the Tracking Aerosol Convection interactions ExpeRiment– Air Quality (TRACER-AQ). This campaign provided a unique opportunity to investigate the fine-scale patterns in NO_2 levels in Houston, TX. One of the devices employed during the TRACER-AQ campaign across its twelve flight days was the GEOstationary Coastal and Air Pollution Events (GEO-CAPE) Airborne Simulator (GCAS) instrument that has been discussed in many previous studies (e.g., Judd et al., 2020; Kowalewski & Janz, 2014; Leitch et al., 2014; Nowlan et al., 2018). The GCAS instrument is an ultraviolet-visible (UV-VIS) spectrometer. Its data is used to retrieve NO_2 columns over a limited number of flight days; this made its observational average more sensitive to meteorological conditions than an instrument with a longer time-record; however, this tool observes NO_2 pattens with uniquely fine-scale resolution (on average 560 x 250 m^2) and performed comprehensive measurements of NO_2

Field Code Changed
Field Code Changed
Field Code Changed
Field Code Changed
Field Code Changed
Field Code Changed
Field Code Changed
Field Code Changed
Deleted: pollution
Field Code Changed
Formatted: Font: Not Italic
Formatted: Font: Not Italic
Deleted: .
Field Code Changed
Field Code Changed
Field Code Changed
Formatted: English (UK)
Deleted: Geostationary Coastal and air pollution events Airborne …
Field Code Changed

columns across large swaths of the city repeatedly up to three time per day. This differs with observations from the TROPOMI instrument on board the Copernicus Sentinel-5 Precursor (S5P) satellite that is in a near-polar sun synchronous orbit (van Geffen et al., 2022) that only observes NO_2 once per day in the early afternoon at a coarser resolution of 3.5 x 5.5 km^2 at nadir. TROPOMI and GCAS spectra are used to retrieve slant NO_2 columns that are converted into vertical columns using an air mass factor (AMF) (Palmer et al., 2001) which is the largest source of uncertainty in the tropospheric vertical column retrieval algorithm (Lorente et al., 2019). Comparing TROPOMI data to other observations – like those from aircraft or ground-based monitors – can serve as a useful diagnostic in characterizing its performance and potential biases. These characterizations have large-scale implications since TROPOMI measures NO_2 columns globally and is useful in areas that lack the observational infrastructure of other instruments. The Pandonia Global Network (PGN) is a network of Pandora instruments (Herman et al., 2009); these instruments are UV-VIS spectrometers that measure spectrally resolved radiance data that is used to retrieve total vertical NO_2 columns. A total of seven Pandora instruments were operational during the TRACER-AQ campaign across three separate sites in and around downtown Houston.

The Comprehensive Air Quality Model with Extensions (CAMx) is a multi-scale photochemical model that can simulate air pollutants including ozone, fine particulate matter, and NO_2 (Ramboll, 2022b). CAMx has been used extensively to investigate Texas air quality by leveraging model input data created by the Texas Commission on Environmental Quality (TCEQ) for air quality planning (Ge et al., 2021; Goldberg et al., 2022) with strong performance compared to remote-sensing column concentrations in Texas (Goldberg et al., 2022; W. Li et al., 2023; Soleimanian et al., 2023). CAMx can be coupled with meteorological models like the Weather Research and Forecasting Model (WRF) which provide the meteorological inputs necessary to simulate fine-scale atmospheric conditions (Jia et al., 2017) – this coupled modeling system is denoted as WRF-CAMx. Fine-scale simulations from WRF-CAMx are useful to understand biases in simulated NO_2 and to identify under- or over-estimates of emissions from sectors and regions in the inventories that drive the model.

In this study, we leverage the unique coincidence of ground-based Pandora spectrometers, high-resolution airborne, and TROPOMI-based remote sensing observations of column NO_2 during the September 2021 TRACER-AQ campaign (Judd et al., 2021). We assess the capabilities of these different data sources through cross-comparisons then compare observed NO_2 to simulated values from a WRF-CAMx simulation to evaluate its performance. Additionally, we consider the impact of different TROPOMI algorithms on performance against Pandora measurements. Our comparisons across the three observational datasets clarifies the range of expected values of NO_2 column concentrations in Houston, TX and characterizes potential deficiencies and biases in observational products and simulated CAMx values. We investigate weekday-weekend performance of the model and consider differences in the spatial distributions of tropospheric NO_2 columns to qualitatively identify the sources that may be under- or overestimated in local inventories and identify the regions in Houston that are most likely impacted by these incorrectly attributed emissions. Additionally, we compare diurnal profiles in column and surface concentrations of NO_2 across relevant products.

Field Code Changed
Field Code Changed
Field Code Changed
Field Code Changed
Field Code Changed
Deleted: TCEQ
Field Code Changed
Field Code Changed
Field Code Changed
Field Code Changed

2 Data and Methods

2.1 Pandora Observations

During the TRACER-AQ campaign a total of seven Pandora instruments operated across three sites in Houston (Table 1). Pandora instruments are ground-based UV-VIS spectrometers that measure spectrally resolved radiances and this work only utilizes those collected via direct-sun observations (Herman et al., 2009). Trace gas spectral fitting routines are employed to characterize column concentrations of gases (e.g., NO_2) similar to remote-sensing and aircraft observations (Judd et al., 2020). Details on the Pandora instruments and their fitting routines are discussed in detail in past studies (Cede, 2021; Herman et al., 2009). The study was designed to have two Pandoras operating coincidently at each site during the campaign; however, due to instrument failures an uneven number of observations were obtained at each site. In order to evenly weigh the observations between the three sites, we select data from a single Pandora instrument at each site. Pan #58 at La Porte, #61 at Aldine, and #25 at University of Houston were chosen for the following reasons. As indicated in Table 1, Pan #61 and Pan #58 clearly have the largest temporal coverage during the TRACER-AQ time period. While Pan #188 measured more frequently at the University of Houston than Pan #25, Pan #188 was operated on a tower about 70 meters above the surface, which results in missing portions of the tropospheric column when operated in direct-sun mode.

Locations of the three sites are presented in Fig. 2F. These three chosen instruments are shaded and bolded in the table below. Pandora direct-sun retrievals represent the "total vertical column" of NO_2 which differs from the aircraft measurements that only measure the tropospheric column. We directly compare these disparate sources by adding a "stratospheric NO_2 column component" derived from TROPOMI estimates to the aircraft measurements (see section 2.2 and 2.3) to compare total column amounts.

Table 1: Details on Pandora instrument operational time

Inst. #	Location	Lat.	Lon.	September 2021 Flight Days with Observations (Number of high- and medium-quality measurements per day)									
				1st	3rd	8th	9th	10th	11th	23rd	24th	25th	26th
11	La Porte	29.67	-95.06	322	347	0	0	0	0	0	0	0	0
58	**La Porte**	**29.67**	**-95.06**	**132**	**190**	**412**	**319**	**415**	**362**	**92**	**439**	**414**	**401**
63	La Porte	29.67	-95.06	0	0	0	0	0	0	0	0	265	207
61	**Aldine**	**29.90**	**-95.33**	**168**	**253**	**400**	**391**	**419**	**367**	**420**	**420**	**405**	**420**
148	Aldine	29.90	-95.33	5	1	3	1	3	3	17	17	10	17
25	**U of H**	**29.72**	**-95.34**	**213**	**256**	**300**	**299**	**392**	**273**	**400**	**382**	**400**	**344**
188	U of H	29.72	-95.34	528	610	1184	957	1137	722	372	749	225	95

Field Code Changed

Field Code Changed

Formatted: Font: Not Italic

Field Code Changed

Deleted: The study was designed to have two Pandoras operating at once during the study. However, this analysis only uses data from a single Pandora at each site. This avoids unevenly weighting observations from sites with fewer or more coincidences that would arise from intercomparisons with airborne, TROPOMI and CAMx datasets and thus we consider the performance equally across all three sites.

Deleted: This avoids unevenly weighting coincidences that would arise from intercomparisons with airborne, TROPOMI and CAMx datasets.

Deleted: 9

Deleted: Aldine

Deleted: La Porte

Deleted: and

Formatted: Font: Italic

Deleted: sites

2.2 GCAS Observations

The GCAS instrument was installed on the NASA G-V aircraft. The GCAS instrument employs charge-coupled device array detectors to observe backscattered light. These data can be used to retrieve column densities of gases like NO_2 below the aircraft using a DOAS computing software (Danckaert et al., 2017). During TRACER-AQ, GCAS collected data over the Houston metropolitan area across 12 days during late August and throughout September 2021. The flight strategy of the aircraft included flying the plane in a 'lawnmower' fashion with flight lines spaced 6.3 km apart, ensuring overlap at flight altitude (FL280) with the instrument field of view of 45 degrees creating one gapless map of NO2 up to three times per flight day. NO_2 observations from GCAS are publicly available at the NASA Atmospheric Sciences Data Center (NASA/LARC/SD/ASDC, 2022). Observations from two of the flight days – a test flight (August 30) and a flight over the Gulf of Mexico (September 27) are excluded from this study because they provided no meaningful data over Houston. Given the relatively short timeframe of flight data collection; meteorological conditions have an influence on the fine-scale patterns in NO_2 columns observations. Owing to this, we summarize some basic conditions and information of the 10 flight days that focused on Houston (Table 2). Wind and meteorological conditions were determined by review of historical weather archives taken at Houston Hobby Airport (NASA, 2023; Weather Underground, 2023).

Field Code Changed

Field Code Changed

Field Code Changed

Table 2: Basic meteorological conditions and notes during GCAS flights

Day of Sept 2021	Day of the Week	High Temp	Wind direction	Additional note
1	Wed	96 F	Weak SW winds	Thunderstorms from S to N, 11 AM to 4 PM
3	Fri	93 F	Weak S winds	Scattered thunderstorms 12 PM to 4 PM
8	Wed	94 F	N turning NE	Clear skies and no rain
9	Thurs	95 F	N turning NE	Afternoon fair weather clouds, no rain
10	Fri	93 F	NE turning E	Clear skies, no rain, some long-range smoke aloft
11	Sat	93 F	E winds	Afternoon fair weather clouds, no rain
23	Thurs	83 F	E winds	Clear skies, no rain, cold font overnight Sept 21
24	Fri	84 F	E turning SE	Clear skies, no rain
25	Sat	87 F	NE turning E	Clear skies, no rain
26	Sun	83 F	Calm then SE	Clear skies, afternoon fair weather clouds

The publicly available GCAS measurements (version R2) include a version of the dataset with reprocessed AMFs to include NO_2 vertical profile estimates from the fine-scale (444 × 444 m^2) WRF-CAMx simulation used in this

analysis (section 2.4). Air mass factors use this vertical profile information to account for altitude-dependent sensitivities in remote-sensing observations. The original vertical profiles in the dataset were derived from a global model, GEOS-CF (Keller et al., 2021), that had a coarser spatial resolution (0.25° × 0.25°). Lastly, to directly compare GCAS measurements to other NO_2 column concentrations we regrid them to a common grid; in this study, we chose the fine-scale WRF-CAMx grid. Only cloud-free GCAS data is considered in this analysis.

To characterize the accuracy and precision of GCAS measurements we compare them to observations from the Pandora instruments (section 3.1). This comparison requires both spatial and temporal screening. Spatially, we restrict our comparison to only the GCAS pixels that contain Pandora instruments. Temporally, we screen out all Pandora measurements that are more than 15 minutes removed from a GCAS overpass and then identify the Pandora measurement time within this 30-minute window that most closely matches the GCAS overpass time. While we choose this 30-minute window as an upper-bound cut-off, 96% and 90% of all Pandora closest matches occur within a 20- and 15-minute window of GCAS overpasses, respectively, indicating that this choice of window will have a minimal impact on our results. After screening the data, we also account for the fact that GCAS only measures the tropospheric component of the NO_2 column. There is a substantial but predictable "above-aircraft" column that is not reflected in the GCAS measurements. This is primarily associated with stratospheric NO_2. To account for this, we approximate the above aircraft component of the GCAS NO_2 columns using the stratospheric NO_2 column component of TROPOMI measurements (section 2.3) and add this to GCAS observations. Additionally, we add a "above aircraft" but below troposphere partial column amount based on the CAMx simulation; we calculate the column. In the 3 highest levels of CAMx that amounts to 0.57 × 10^{15} molecules cm^{-2} and add this amount to GCAS.

2.3 TROPOMI Observations

The TROPOMI instrument – on board the Sentinel-5P satellite – has measured total slant columns of NO_2 daily at approximately 13:30 local time globally from April 30, 2018 to present (European Space Agency, 2021). The slant column measurements were converted into tropospheric vertical column amounts by subtracting off a stratospheric NO_2 component and transforming the remaining tropospheric slant column to vertical column using an air mass factor. We download the publicly available data (https://data-portal.s5p-pal.com/products/no2.html; https://dataspace.copernicus.eu/) coincident with the TRACER-AQ campaign in September 2021 for overpasses of Houston, TX. In this study, we primarily consider measurements from the latest version (2.4.0) (Eskes et al., 2023); however, we additionally consider measurements processed using the version 2.3.1 algorithm (van Geffen et al., 2021) and the NASA Multi-Decadal Nitrogen Dioxide and Derived Products from Satellites (MINDS) product (Lamsal et al., 2022) and intercompare these different versions (Fig. 3). All product versions stem from the same slant column retrieval but differ in the calculation of the air mass factor for slant to vertical column conversions, and in the case of NASA MINDS, separation of the stratosphere and troposphere (Bucsela et al., 2013). The main difference between 2.3.1 and 2.4.0 is the use of the 0.125° × 0.125° Directional Lambertian Equivalent Reflectivity (DLER) climatology derived from TROPOMI observations which replaces an old 0.5° × 0.5° Lambertian Equivalent

Deleted: publicly available d
Field Code Changed
Deleted: ¶
Formatted: Space Before: Auto, After: Auto
Deleted:
Formatted: Font: Not Italic
Deleted: Spatially, we identify the CAMx grid cell in which each Pandora instrument is located and only consider GCAS measurements that were regridded to these grid cells.
Deleted: bias correction factor
Deleted: correction factor
Deleted: constant correction factor
Deleted: PM
Field Code Changed
Deleted: are be
Field Code Changed
Field Code Changed
Field Code Changed
Field Code Changed
Field Code Changed
Field Code Changed

Reflectivity (LER) dataset used in v2.3.1 (Eskes et al., 2023). NASA MINDS uses a geometry-dependent surface Lambertian Equivalent Reflectivity (GLER) product for their surface reflectivity input into the AMF calculation based on MODIS observations. The other main difference in these products include use of different a priori NO_2 profiles (1° × 1° TM5-MP for v2.3.1 and v2.4.0 vs 0.25° × 0.25° GMI simulation for NASA MINDS). A comparison between TROPOMI version 2.4.0 and a MAX-DOAS network found that in moderately polluted locations TROPOMI had a median bias of -35%; a comparison between TROPOMI version 2.4.0 and PGN found a median bias of -18% over polluted stations (Lambert et al., 2023).

These publicly available TROPOMI data are further processed for this study. We screen TROPOMI measurements to consider cloud coverage and erroneous data using the recommended qa_value filter (> 0.75). We regrid the TROPOMI NO_2 observations (resolution of 3.5 x 5.5 km^2 at nadir) onto the WRF-CAMx grid (444 × 444 m^2). When comparing TROPOMI observations to Pandora instruments we follow the same spatial and temporal screening approach as discussed for GCAS. Spatially, we identify the CAMx grid cell in which each Pandora instrument is located and only consider TROPOMI measurements that were regridded to these grid cells. Temporally, we screen out all Pandora measurements that are more than 15 minutes removed from a TROPOMI overpass time and then identify the Pandora measurement time within this 30-minute window that most closely matches the TROPOMI overpass time. While we choose this 30-minute window as an upper-bound cut-off, 100% and 97% of all Pandora closest matches occur within a 20- and 15-minute window of TROPOMI overpasses, respectively, indicating that this choice of window will have little impact on our results. Using WRF-CAMx vertical profile information we calculate both a total and tropospheric NO_2 column from TROPOMI v2.4.0 measurements using new AMF derived from the WRF simulation and we difference the total and tropospheric values to calculate a stratospheric NO_2 column component from TROPOMI. We take the spatial and temporal average of this stratospheric component in Houston during the TRACER-AQ campaign to calculate a constant bias correction to convert tropospheric NO_2 columns – from GCAS and WRF-CAMx – to quasi-total NO_2 columns when comparing them to total NO_2 column measurements from Pandora instruments. This stratospheric vertical column NO_2 amount of 3.0×10^{15} is typical for Houston during summer (Geddes et al., 2018). Boersma et al. (2018) suggests that 0.5×10^{15} molecules cm^{-2} is the upper limit of structural uncertainty in the stratospheric estimate; this uncertainty should be considered when reviewing results that compare total column amounts (i.e., results comparing GCAS and CAMx to Pandora). We additionally account for diurnal variation in the stratospheric column by applying the results from work by K.-F. Li et al. (2021); they calculate a daytime stratospheric NO_2 column increase rate of 1.34×10^{14} molecules cm^{-2} starting at 7:00 LT. We apply this increase rate by calculating the difference in hours between the dataset times – either the GCAS overpass times or CAMx simulation hours – and 13:30 – the approximate TROPOMI overpass time – and then multiply this difference by the increase rate. In doing so, total column values before the TROPOMI overpass are decreased and total column values after the overpass are increased.

Field Code Changed
Deleted: ,
Field Code Changed
Formatted: Font: Not Italic
Deleted: (Geddes et al., 2018).
Deleted: (
Formatted: Font: Not Italic
Deleted: agrees well with a previous study
Field Code Changed
Deleted: ,
Deleted: that found that stratospheric NO_2 in the southeastern US – on a single day in February 2005 – was approximately 2×10^{15} molecules cm^{-2}. This study also
Field Code Changed
Field Code Changed
Deleted: (
Deleted: ,

2.4 WRF-CAMx simulated NO_2

For this study, a set of simulations were conducted employing version 4.3.3 of the Advanced Research Weather Research and Forecasting (WRF) model (Skamarock et al., 2021) jointly with the Comprehensive Air Quality Model with Extensions (CAMx) v7.20 with the CB6r5 chemical mechanism for a simulation period that matched the September 2021 TRACER-AQ timeframe. A new high-resolution modeling platform was designed specifically for this study that adopted prior approaches used in Texas Commission on Environmental Quality (TCEQ) state implementation plan (SIP) modeling (TCEQ, 2021) to update emissions.

The WRF model is a mesoscale numerical weather prediction system designed to serve both operational forecasting and atmospheric research needs (Skamarock et al., 2005, 2008). We define the WRF modeling domains as slightly larger than the corresponding CAMx domains (Fig. 1) to avoid possible numerical artifacts near domain boundaries when transferring WRF meteorology to CAMx. The 36 km CAMx domain (red) includes the continental US, Mexico, and parts of Central America and Canada. The 36 km, 12 km (blue) and East Texas 4 km (green) domains are also used by the TCEQ for State Implementation Plan (SIP) modeling. The higher resolution domains (1.333km (orange) and 0.444km (cyan)) were selected to include the most relevant GCAS flight tracks while considering computational expense.

Deleted: ARW

Field Code Changed

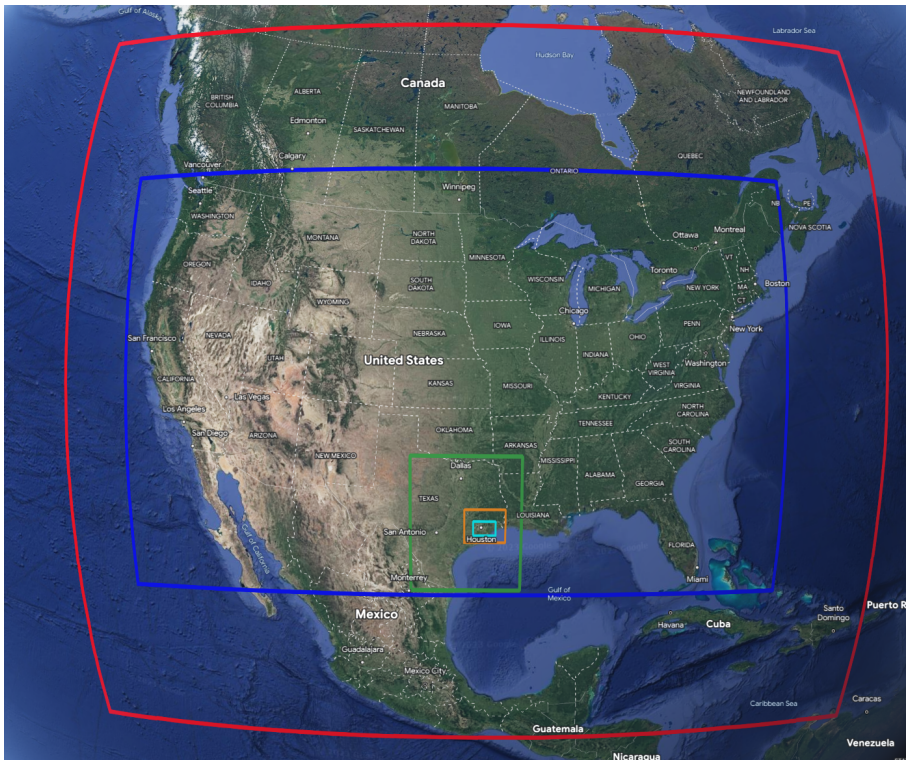

290

Figure 1: Modeling domains used in the CAMx simulation for the 36 km resolution (red), 12 km resolution (blue), 4 km resolution (green), 1.333 km resolution (orange), and the 0.444 km resolution (cyan). Maps data provided by Google © 2020, Landsat / CopernicusData SIO, NOAA, U.S. Navy, NGA, GEBCO, IBCAO,
295 **INEGI, and U.S. Geological Survey.**

Field Code Changed

Additional information on the WRF-CAMx modeling is included in the supplemental including the WRF physics options (Table S1), vertical layer mapping from WRF to CAMx (Table S2), and CAMx science options (Table S3). We used 0.25° Global Forecasting System (GFS) data assimilation system (GDAS) analysis data (DOC/NOAA/NWS/NCEP/EMC, 2023) as initial conditions for the WRF meteorological model; this GDAS data is
300 also used for boundary conditions and data assimilation. We configured the output timesteps of WRF to 15 minutes for the higher resolution domains. Conducting WRF simulations at fine spatial resolutions (i.e., 4 km, 1.333 km, and 0.444 km) requires careful consideration of physical schemes that are sensitive to grid spacing. We turn off the convective cumulus parametrization scheme for the fine grids because WRF can explicitly simulate convection for them. For coarser grids we turn on the cumulus parametrization to account for sub grid-scale convection. The other

Field Code Changed

physics options (Table S1) are kept consistent across the different resolutions. The CAMx simulation was first performed over the coarser domains (36 km, 12km, and 4 km) from which initial and boundary conditions were extracted for the higher resolution domains. TCEQ developed the 2019 modeling emissions inventory for the Dallas-Fort Worth (DFW) and Houston-Galveston-Brazoria (HGB) Attainment Demonstration (AD) SIP revisions (TCEQ, 2021). Starting with this inventory we implement further changes as discussed in the next paragraph.

First, we update the CAMx modeling emissions inventory from the TCEQ platform to incorporate 2021 hourly Continuous Emissions Monitoring Systems (CEMS) (EPA, 2023) data for the eleven major electric generating units (EGUs) listed in Table S4. We download hourly data from Clean Air Markets Program Data (CAMPD) for the eleven EGUs for the August 30-Sep 27, 2021, period and stack parameters were based on the TCEQ 2019 emissions platform (TCEQ, 2021). Second, we update shipping emissions to incorporate MARINER v2 (Ramboll, 2022a) emissions built with 2021 Automatic Identification System (AIS) data for the higher resolution domains. Third, we reprocess link-based on-road mobile emissions for the higher resolution domains. Fourth, we update biogenic emissions and lightning NO_X (LNO_X) based on WRF meteorology. Specifically, we use the Model of Emissions of Gases and Aerosols from Nature (MEGAN) (Guenther et al., 2012) version 3.2 for biogenic emissions, the Fire Inventory of NCAR (FINN) version 2.2 (Wiedinmyer et al., 2011) for fire emissions, and lightning NO_X emissions derived by applying the CAMx LNO_X processor to the 2021 meteorological data from the WRF simulation. Considering that wildfires in the Houston area are rare and that LNO_X emissions are associated with convective clouds that obscure remote sensing column observations, we excluded these two emission sources from the finer resolution domains (the 1.333 and 0.444 km domains) but included them in the larger domains. These two sources represent a small fraction of emissions in the local Houston area that is the primary focus of the finer resolution simulations. Lastly, we regrid all other gridded emissions from the coarser domains to the high-resolution domains without refining their spatial resolution. Specifically, all point sources are geo-located to the grid cell containing the source. On-road mobile source emissions and shipping emissions were provided for individual links which we allocated to 444 m grid cells, and are based on known roadway networks, ship tracks, and traffic patterns. Airport and railyard emissions were allocated to 444 m grid cells within the property boundary. Other sources retained the 4 km grid resolution provided by the TCEQ. Daily emissions of NO_X and volatile organic compounds (VOCs) in tons per day (tpd) for a September weekday are presented in Table 3 below.

We evaluate the WRF simulation meteorology by comparing surface-level wind speed, direction, temperature, and water vapor mixing ratio to observations from sixteen ground-level monitors (Table S5-8 and Fig. S2-11) and calculate the mean bias error (MBE), mean absolute error (MAE), and Pearson-R squared (R^2) statistics as defined in supplement table S2. Circular statistics are calculated using the Astropy circular statistics module for Python (The Astropy Collaboration, 2022). We obtain integrated surface data from NCDC in the DS3505 format (ftp://ftp.ncdc.noaa.gov/pub/data/noaa/); these data consist mainly of airport locations and have good meteorological siting and quality assurance procedures.

Deleted: Reasonable Further Progress (RFP)
Field Code Changed
Deleted: ¶
Formatted: Space Before: Auto, After: Auto
Field Code Changed
Deleted: EGUs …lectric generating units (EGUs) listed in Table S4. We download hourly data from Clean Air Markets Division … [1]
Field Code Changed [2]
Deleted: NO_x …O_X (LNO_x [3]
Field Code Changed [4]
Deleted: NO_x …O_X emissions derived by applying the CAMx LNO_x …NO_X processorr[2] [5]
Formatted: Font: Not Italic
Deleted: lightning nitrogen oxides (
Formatted: Font: Not Italic
Deleted: x
Deleted:)
Formatted: Font: Not Italic
Deleted: would
Formatted: Font: Not Italic
Deleted: Considering the limited extent of the high-resolution CAMx domains and large degree of uncertainty with both the fire and LNOx emissions, we excluded these two emission sources from the finer resolution domains
Formatted [6]
Deleted: NO_x …O_X and VOC …olatile organic compounds (VOCs) in tons per day (tpd) for a September weekday are presented in Table 3 below.¶ [7]
Deleted: ¶
Formatted [8]
Field Code Changed
Deleted: et al.
Formatted: Font: Not Italic
Field Code Changed
Formatted [9]

Generally, meteorological conditions simulated by WRF agree with ground-level observations especially on the more data rich non-cloudy days that are the most important for our intercomparison. Across all days, the WRF wind direction MBE was -8°, wind speed MBE was -0.02 m/s, temperature MBE was 0.39 K, and water vapor mixing ratio MBE was -1.45 g/kg. Across the eight non-cloudy days, hourly and site-specific – across the sixteen monitors – WRF wind direction (R^2=0.3 to 0.8; MAE=14° to 32°), wind speed (R^2=0.1 to 0.5; MAE=0.94 m/s to 1.35 m/s), temperature (R^2=0.69 to 0.81; MAE=0.93 K to 1.18 K), and water vapor mixing ratio (R^2=0.28 to 0.78; MAE=0.87 g/kg to 3.11 g/kg) performed moderately compared to observations given the fine spatial and temporal resolution. Additionally, we compare simulated hourly NO_2 (Fig. S12) and maximum daily eight-hour average or "MDA8" O_3 (Fig. S13) to observations from seventeen TCEQ continuous air monitoring stations (CAMS) operating in Houston. We find poor performance and a strong negative bias in the simulated surface-level NO_2 (NMB=-59%) and generally good performance in the simulated surface-level MDA8 O_3 (NMB=-2.5%) compared to observations.

Formatted: Font: Not Italic

Formatted: Font: Not Bold

Formatted: Font: Not Bold

Formatted: Font: Not Italic

Formatted: Font: Not Italic

Deleted: We evaluate the WRF simulation meteorology by comparing surface-level wind speed, direction, temperature, and relative humidity to observations from sixteen ground-level monitors (Supplemental Tables X and Figures Y). We obtain integrated surface data from NCDC in the DS3505 format (ftp://ftp.ncdc.noaa.gov/pub/data/noaa/); these data consist mainly of airport locations and have good meteorological siting and quality assurance procedures. Generally, meteorological conditions in the WRF simulation agree with ground-level observations especially on the more data rich non-cloudy days that are the most important for our intercomparison.¶

Table 3: CAMx 444 × 444 m² domain-wide summary of average September weekday emissions by sector in units of tons per day (tpd).

Emission Sector	Spatial Resolution	NO_X (tpd)	VOC (tpd)
EGUs	Point locations	25.5	0.2
On-road mobile	Line source	70.9	34.7
Railyards	444 m gridded	4.2	0.3
Shipping	Line source	63.9	4.3
KIAH airport	444 m gridded	6.4	0.8
KHOU airport	444 m gridded	1.8	0.4
Other			
Off-road mobile	4 km gridded	33.1	31.4
Non-EGU Point Sources	Point locations	47.9	27.8
Oil and Gas	4 km gridded	0.2	0.0
Area	4 km gridded	92.8	623.2
MEGAN biogenic	444 m gridded	25.9	319.7

Deleted: NO_x

Formatted Table

Deleted: *

2.5 Diurnal Comparison

We further intercompare these data by grouping them at locations and then calculating their average diurnal profiles during the TRACER-AQ campaign for both column and surface-level NO_2. Specifically we compare GCAS, CAMx, Pandora, and GEOS-CF (Keller et al., 2021) NO_2 columns at the three Pandora sites during TRACER-AQ flight days. We include NO_2 data from GEOS-CF – that will be used for processing NO_2 remote-sensing observations from the NASA Tropospheric Emissions: Monitoring of Pollution (TEMPO) mission – to characterize differences between a global simulation and our regional WRF-CAMx modeling. Simulated surface and NO_2 columns from GEOS-CF are obtained through the GMAO OPeNDAP interface (https://opendap.nccs.nasa.gov/dods/) for all of 2021 and filtered to the specific Pandora instrument locations and during TRACER-AQ flight days. We apply both spatial and temporal screening. Spatially, we identify the CAMx grid cell – for GCAS and CAMx – and GEOS-CF grid cell in which the Pandora instrument is located. Temporally, for GCAS, we round all overpass times to the nearest hour and calculate the median value for each hour across all overpasses and days. For CAMx, GEOS-CF, and Pandora we identify the simulated and observed NO_2 column concentration closest to the hour and calculate the median value across all flight days and locations.

Formatted: Indent: First line: 0", Space Before: Auto, After: Auto

Field Code Changed

Formatted: Font: Not Italic

Deleted: We include NO_2 data from GEOS-CF to characterize differences between a global simulation and our regional WRF-CAMx modeling.

Deleted:

Deleted:

Deleted: ¶

For diurnal comparisons at the surface, we use surface-level NO_2 concentrations from CAMx and GEOS-CF and apply the same temporal screening. Spatially, for the surface-level we consider concentrations at a point in between the three Pandora instruments that is representative of downtown concentrations (29.7 °N, 95.3 °W). We choose this point to represent the temporal behavior of the wider regions rather than individual sites. Additionally, we download

hourly NO_2 concentrations from the US Environmental Protection Agency (EPA) Air Quality System (AQS) (https://aqs.epa.gov/aqsweb/airdata/download_files.html). We download all hourly data for 2021 for the US and filter the TRACER-AQ flight days and for monitors in Harris County. We identify the median hourly concentrations across these monitors and the TRACER-AQ flight days.

3 Results

3.1 Comparisons to Pandora Observations

The observations from ground-based Pandora instruments are considered the most accurate of all observational platforms measuring column NO_2 presented in this project due to low uncertainties in their air mass factors (Herman et al., 2009) when operating in direct-sun mode. The air mass factor in this mode is calculated from simple solar geometry – unlike TROPOMI and GCAS, which rely on a priori assumptions like the vertical NO_2 profile and surface reflectivity. Pandora AMFs are not reliant on an a priori profile as the data we are using is only in direct-sun mode in cloud-free scenes. AMF for Pandora is analogous to pathlength through the atmosphere relative to the vertical path. Since all the signal is from direct sun path (extremely minimal scattering), this is purely geometric. Given this, we use Pandora observations as our reference dataset to characterize the performance of the two observational datasets – GCAS and TROPOMI – along with the WRF-CAMx simulation across three sites (Table 1). These three sites (Aldine, La Porte, and University of Houston) are located in the heavily polluted inner region of Houston that we denote as "urban Houston" (Fig. 2F). Background observations from Pandora instruments in less polluted sites were unavailable during the TRACER-AQ campaign so there is less certainty about the performance of GCAS, TROPOMI, and CAMx outside of urban Houston. We consider the performance of GCAS processed with a CAMx-based AMF (Fig. 2A), TROPOMI processed with a CAMx-based AMF (Fig. 2B), and CAMx (Fig. 2C) and the performance of GCAS and TROPOMI with the operational AMFs (Fig. 2D and 2E) individually and then intercompare the three datasets across the ten GCAS observation days (Fig. 2G).

When comparing the observational and simulated datasets to Pandora observations we consider the total column NO_2 – we add a stratospheric component from TROPOMI to the tropospheric column NO_2 of GCAS and CAMx to total column as discussed in the methodology. For TROPOMI, we use an AMF derived from the CAMx simulation to calculate a tropospheric NO_2 column from TROPOMI; following the TROPOMI users guide, we multiply the total averaging kernel by the ratio of the total air mass factor to the tropospheric air mass factor. We difference the total column NO_2 from TROPOMI with the tropospheric column to estimate a constant stratospheric NO_2 column amount that we add to GCAS and CAMx when we compare them to Pandora; this corresponds to a mean value of 3.0×10^{15}. For GCAS, we apply an additional amount to account for the NO_2 column in the upper troposphere – above the aircraft and below the tropopause. We calculate the column of levels 27-29 that correspond to 9400-18100 m above sea-level – that extends roughly from the height that GCAS flies at of around 9100 m to the tropopause – and apply this to the GCAS results; this corresponds to a value of 0.57×10^{15} molecules cm^{-2}. For all results that

Field Code Changed
Field Code Changed
Deleted: i
Formatted: Font: Not Italic
Formatted: Font: Not Bold
Deleted: bias correct
Deleted: Specifically
Formatted: Font: Not Italic
Deleted: the
Formatted: Font: Not Italic
Formatted: Font: Not Italic
Formatted: Font: Not Italic
Deleted: correction factor
Formatted: Font: Not Italic
Deleted: apply
Formatted: Font: Not Italic
Formatted: Font: Not Italic
Formatted: Font: Not Italic
Formatted: Font: Not Italic
Deleted: correction factor
Formatted: Font: Not Italic
Formatted: Font: Not Italic
Formatted: Font: Not Italic
Deleted: 42
Formatted: Font: Not Italic
Formatted: Font: Not Italic
Formatted: Font: Not Italic
Formatted: Font: Not Italic
Deleted: We apply this same correction factor to CAMx.

include comparison to Pandora we present total NO_2 columns; for results where we only intercompare GCAS, TROPOMI, and CAMx we compare the tropospheric column. All statistical measures (e.g., R^2) are defined in the supplement.

Formatted: Font: Bold, Not Italic

Deleted: We define all statistics that are mentioned in the results and discussion in the supplement. ¶

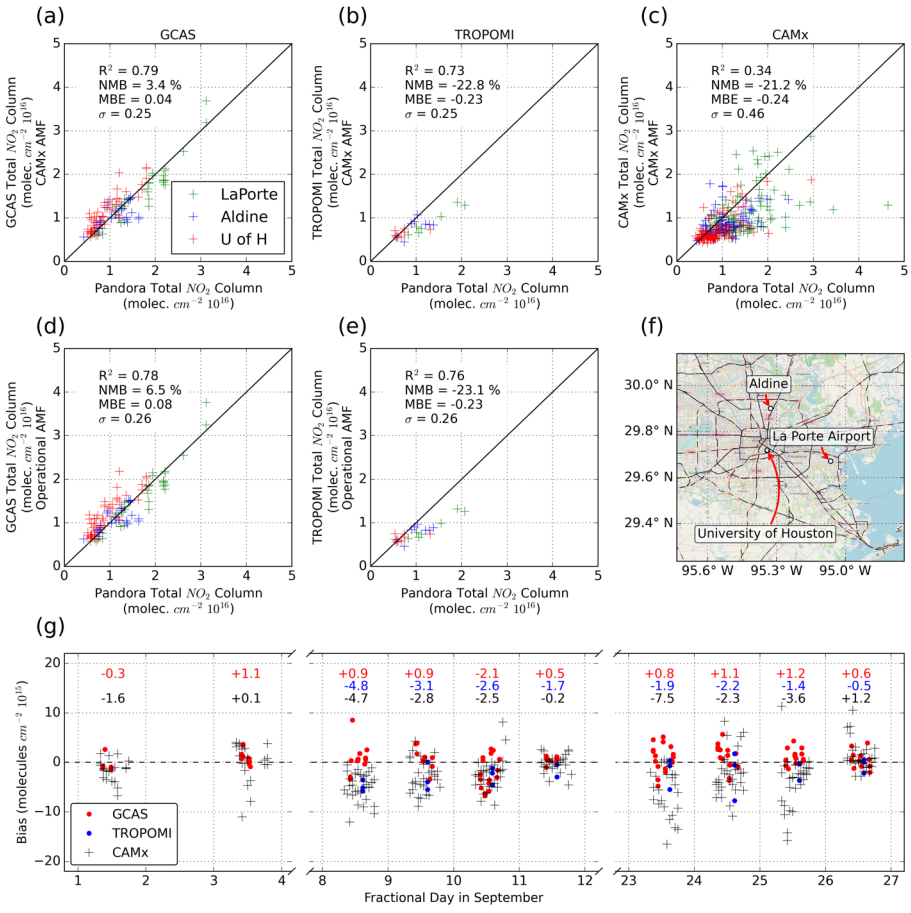

Figure 2: Comparison of Pandora total column NO_2 to GCAS using CAMx-based AMFs (A), TROPOMI v2.4.0 using CAMx-based AMFs (B), and CAMx (C) and GCAS (D) and TROMPOMI v2.4.0 (E) with their operational AMFs. Tropospheric columns from GCAS and CAMx are bias corrected with a TROPOMI-derived stratospheric column factor as discussed in the methodology. Data from all possible overpasses

Field Code Changed

coincident within 15 minutes of a Pandora observation are considered. GCAS flight times generally ranged from 8:00 AM-4:00 PM CDT. TROPOMI overpasses occurred around 1:30 PM local time. Color coding indicates which of the Pandora instruments NO_2 column concentrations are being compared against indicated in the legend in subplot A, but statistics are presented across all locations. Map of Pandora instrument sites in urban Houston (F). Bias between the three datasets and Pandora across GCAS flight days (G) with the overall average daily bias indicated above the points for all three datasets. The data are color coded based on the observed or simulated source that is being compared against Pandora measurements. © OpenStreetMap contributors 2023. Distributed under the Open Data Commons Open Database License (ODbL) v1.0.

In Fig 2A-C we characterize the performance of the observational and simulated datasets of NO_2 column concentrations across the three sites in Houston. For each of the GCAS flight days, we compare GCAS and TROPOMI observation against Pandora measurements for every overpass that was not obstructed by cloud coverage; for CAMx we compare simulated columns for every daytime hour of each GCAS flight day.

Observations from GCAS were both well correlated (r^2=0.79) and slightly high biased (NMB=+3.4%) when compared to measurements from Pandora. Use of the CAMx AMF in place of the operational AMF had a minimal impact on comparisons to Pandora (from r^2=0.78 and NMB=+6.5%). Observations from TROPOMI on GCAS flight days were also well correlated with Pandora measurements (r^2=0.73) but there was a negative bias (NMB=-22.8%) in v2.4.0. This bias was worse for more NO_2 polluted scenes. This negative bias may be attributable to the coarser resolution of TROPOMI compared to GCAS that weakens its ability to capture fine-scale plumes (Wagner et al., 2023) of NO_2 associated with road systems, airports, power stations, and industrial facilities. Similar to GCAS, use of the CAMx AMF in place of the operational AMF for TROPOMI had a minimal impact on comparisons to Pandora (from r^2=0.76 and NMB=-23.1%).

We calculate the ratios of the TROPOMI v2.4.0 product with the CAMx AMF compared to the operational AMF (Fig. S1) in September 2021 throughout the domain and note that tropospheric column NO_2 increases in the urban core and decreases in the city outskirts. The areas with Pandora instruments – in suburban Houston – have roughly equivalent values. Given that Pandora instruments were not located at either the most or least polluted areas of the metropolitan area, the benefit of the CAMx AMF may be underrepresented by our findings at the Pandora sites.

We compare simulated NO_2 columns from CAMx with Pandora measurements; however, in this comparison there are more points to intercompare as columns were simulated for each hour of every flight day by CAMx and observed multiple times per hour from Pandora. The CAMx simulated columns were less correlated with Pandora measurements (r^2=0.34) than compared to TROPOMI and GCAS, and they had a consistent negative bias (NMB=-21.2%). This poor correlation could partially be explained by differences in WRF simulated meteorology and observed meteorology specifically from differences in wind speed and direction and an inability to fully capture the bay breeze in Houston. We generally find good agreement in the WRF simulated meteorology (Table S5-S8 and Fig

Deleted: 80
Deleted: minimally
Deleted: 0
Deleted: 1
Deleted: negligible impact
Deleted: 9
Deleted: 3
Deleted: 2
Deleted: Similar to GCAS, observations from TROPOMI were slightly affected by the new CAMx AMF (from r^2=0.76 and NMB=-23.1%) with a slight degradation improvement in correlation and slight improvement degradation in bias.
Field Code Changed
Deleted: t
Deleted: ; however, in rural areas the CAMx AMF has a greater impact on TROPOMI NO_2 columns
Deleted: 4
Deleted: 5
Deleted: 5
Formatted: Font: Not Italic
Formatted: Font: Not Italic
Deleted: Supplemental
Deleted: X
Deleted: ure

S2-11); however, the non-systematic differences in wind direction on the order of 20° would likely degrade correlation between observed and simulated NO_2 columns. We do not find notable differences in correlation or error on windier days than on calmer days (Table S5-S6). Given that there is no apparent systematic bias in the meteorology, the negative bias in NO_2 columns is likely attributable to an underestimate of NO_x emissions. Additionally, there can be substantial differences in vertical mixing coefficients in different schemes in the models, and these can impact the biases in column concentrations (de Foy et al., 2007; Riess et al., 2023).

In Fig. 2G, we intercompare the daily variability in biases across the ten GCAS flight days. There were no TROPOMI data for the first two flight days because cloud coverage blocked TROPOMI observations at the Pandora sites during its overpass time. The daily average bias of GCAS observations were consistently small throughout the entire period: they ranged from -2.1 to +1.2 molecules cm^{-2} 10^{15} on September 10th and the 3rd and 24th, respectively. TROPOMI observations were consistently biased systematically low: they ranged from -4.8 to -0.5 molecules cm^{-2} 10^{15}; however, on all days except the 26th daily averaged TROPOMI biases were more negatively biased than -1.3 molecules cm^{-2} 10^{15} compared to Pandora measurements. Unlike the two observational datasets, the bias in simulated CAMx NO_2 columns had much higher daily variability. On some days, such as September 3rd, there was little bias in simulated columns compared to Pandora measurements, and on other days such as September 26th, there was a minor high bias (+1.2 molecules cm^{-2} 10^{15}); however, on most days there was a negative bias that was the strongest on September 23rd when NO_2 columns were biased as low as -7.5 molecules cm^{-2} 10^{15}. Generally, simulated CAMx columns perform better on weekend days (11th, 25th, and 26th) which is investigated in greater detail in section 3.4.

Deleted: Y

Formatted: Font: Not Italic

Formatted: Font: Not Italic

Deleted: x

Formatted: Font: Not Italic

Deleted: ¶

Deleted: This poor correlation could partially be explained by differences in WRF simulated meteorology and observed meteorology specifically from differences in wind speed and direction and an inability to capture the bay breeze in Houston. The negative bias is likely attributable to an underestimate of NOx emissions, but it could also be partially due to an incorrect effective NO_2 lifetime driven by the nonlinear interactions of chemistry and dispersion.

Field Code Changed

Deleted: 6

Deleted: 0

Deleted: 8

Deleted: -

Deleted: 0

Deleted: .

Deleted: 7

Deleted: 8

Deleted: 0

3.2 Comparisons of different TROPOMI algorithms to Pandora Observations

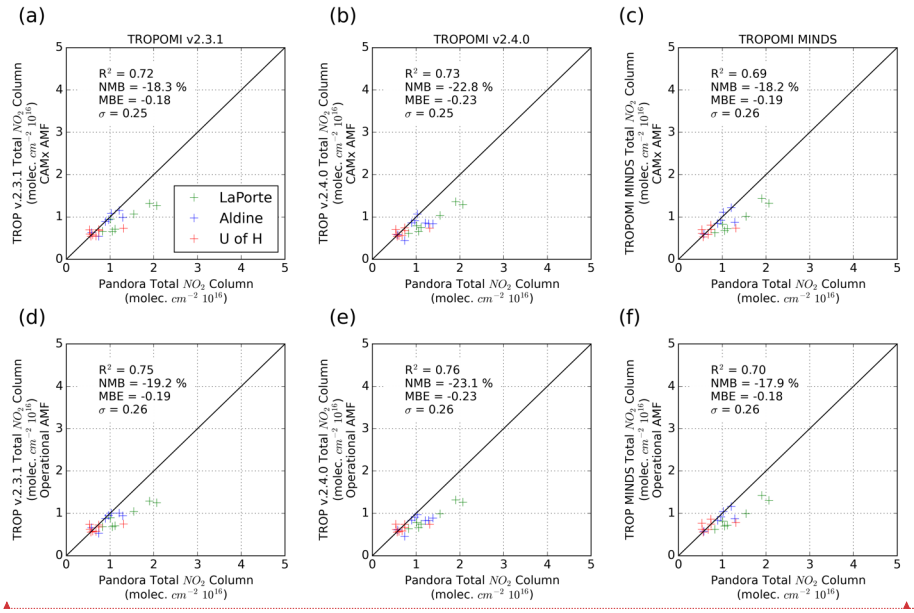

Figure 3: Comparison between Pandora measurements and TROPOMI observations using the CAMx AMF for version 2.3.1 (A), 2.4.0 (B), and NASA MINDS (C) and the same respective versions using the operational AMF (D-F). Data from all possible overpasses coincident within 15 minutes of a Pandora observation are considered with one exception: data from September 11th, 2021, was missing from the NASA MINDS product and so values in plots C and F exclude this day.

We intercompare TROPOMI observations to Pandora measurements across three different algorithms: version 2.3.1 (Fig. 3 A, D), version 2.4.0 (Fig. 3B, E), and the NASA MINDS product (Fig. 3C, F) using both the CAMx AMF (top row) and the Operational AMF (bottom row) for the same Pandora instruments in Houston during the TRACER-AQ Campaign. Overall, the choice of algorithm and AMF does affect the performance of TROPOMI compared to Pandora, albeit slightly. Regardless of AMF, version 2.4.0 appears to have the worst normalized mean bias in Houston during TRACER-AQ (r^2=0.73, and NMB=-22.8%), version 2.3.1 is improved (r^2=0.72 and NMB=-18.3%) while the NASA MINDS product performs comparably (r^2=0.69 and NMB=-18.2%) to version 2.3.1. Notably, NASA MINDS data for September 11th are missing so these data are excluded from panels C and F. For version 2.3.1 and version 2.4.0 the CAMx AMF slightly improves the bias; however, for the MINDS product the CAMx AMF slightly worsened bias compared to the operational AMF. The correlation is generally unaffected by the

Formatted: Font: (Default) Times New Roman

Formatted: Font: (Default) Times New Roman

choice of AMF. We choose TROPOMI version 2.4.0 for the intercomparison in the following sections as it is the most recent version.

3.3 Comparisons of GCAS, TROPOMI, and CAMx data on the CAMx grid

The comparisons between Pandora measurements and the datasets indicate that GCAS observations are in best agreement with Pandora. While TROPOMI performs worse than GCAS, it still decisively outperforms simulated NO_2 columns from CAMx at Pandora sites in both correlation and bias despite its coarser resolution. With the above in mind, in this section we present NO_2 columns observed from GCAS and TROPOMI and simulated from CAMx at the 444×444 m^2 resolution of the CAMx grid. We extend the prior comparison beyond focusing on three discrete points in urban Houston to the entire CAMx domain to get a more complete picture of the spatial components of these datasets. For each dataset we consider observations across all ten GCAS flight days. We begin by comparing GCAS observations only with CAMx simulated columns across all GCAS overpasses as these data are less limited temporally than TROPOMI observations (Fig. 4).

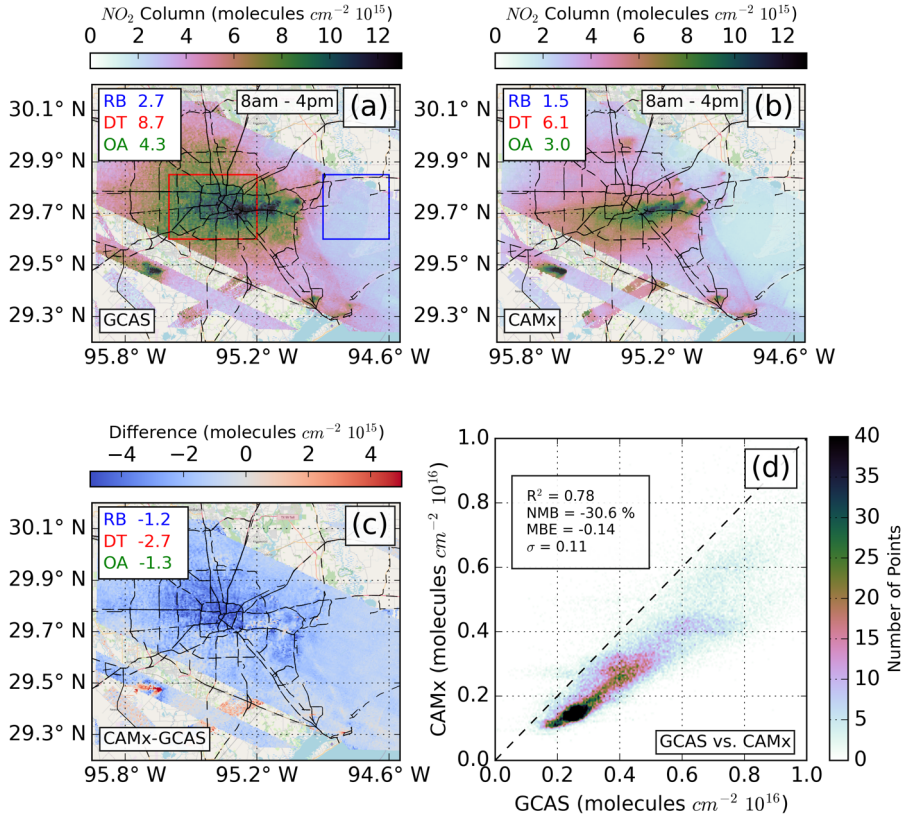

Figure 4: Comparison of GCAS observations to CAMx simulated NO_2 columns across all data during GCAS overpasses (generally 8 am – 4 pm). Temporally averaged GCAS NO_2 columns (A), temporally averaged simulated CAMx NO_2 columns (B), the absolute difference between GCAS and CAMx (C), and a scatter density plot comparing all observations between GCAS and CAMx (D). We identify three distinct areas: downtown or "DT" (red), the low emissions East Galveston rural Bay or "RB" (blue), and all other areas or "OA" (green) and calculate the averages in the top left of each chart. © OpenStreetMap contributors *2023*. Distributed under the Open Data Commons Open Database License (ODbL) v1.0.

When considering data from all GCAS overpasses (Fig. 4A, B, C) we observe a consistent negative bias in the CAMx product compared to GCAS observations throughout the domain that worsens in the downtown (DT) area (-2.7

Deleted: 3

molecules cm^{-2} 10^{15}) compared to background levels in the rural East Galveston Bay (RB) (-1.2 molecules cm^{-2} 10^{15}). Near the W A Parish power station in the southwestern area of the domain there are a mixture of positive and negative biases in the CAMx simulated columns that are likely indicative of errors in wind speeds or directions in the CAMx simulation. Overall, the CAMx simulated columns were well correlated with GCAS observations (r^2=0.78) but the negative bias was substantial (NMB=-30.6%) (Fig. 4D).

We continue this comparison in Fig. 5 where we limit the GCAS and CAMx values temporally around TROPOMI overpasses. For Fig. 5, we screen out all observations that are +/- 90 minutes from TROPOMI overpass for each day and then temporally average the observations across the GCAS flight days (Fig. 5A-C). We difference, both absolutely (Fig. 5D-F) and relatively (Fig. 5G-I), the three pairs of datasets and present them in scatter density plots (Fig. 5J-L). We focus on three regions: downtown Houston (DT) (red), the rural East Galveston Bay (RB) (blue), and all other areas (OA) (green) and calculate the mean values and differences for these areas in the top left of each of the plots. The results presented in Fig. 5 are the temporal average across all flight days; however, similar figures for individual flight days are presented in the supplemental (Fig. S14-23)

Deleted: -
Deleted: 0
Deleted: 8
Deleted: -
Deleted: 9
Deleted: 23
Deleted: 8
Deleted: (DT)
Deleted: (RB)
Deleted: (OA)
Deleted: 2
Deleted: 1
Deleted: 1

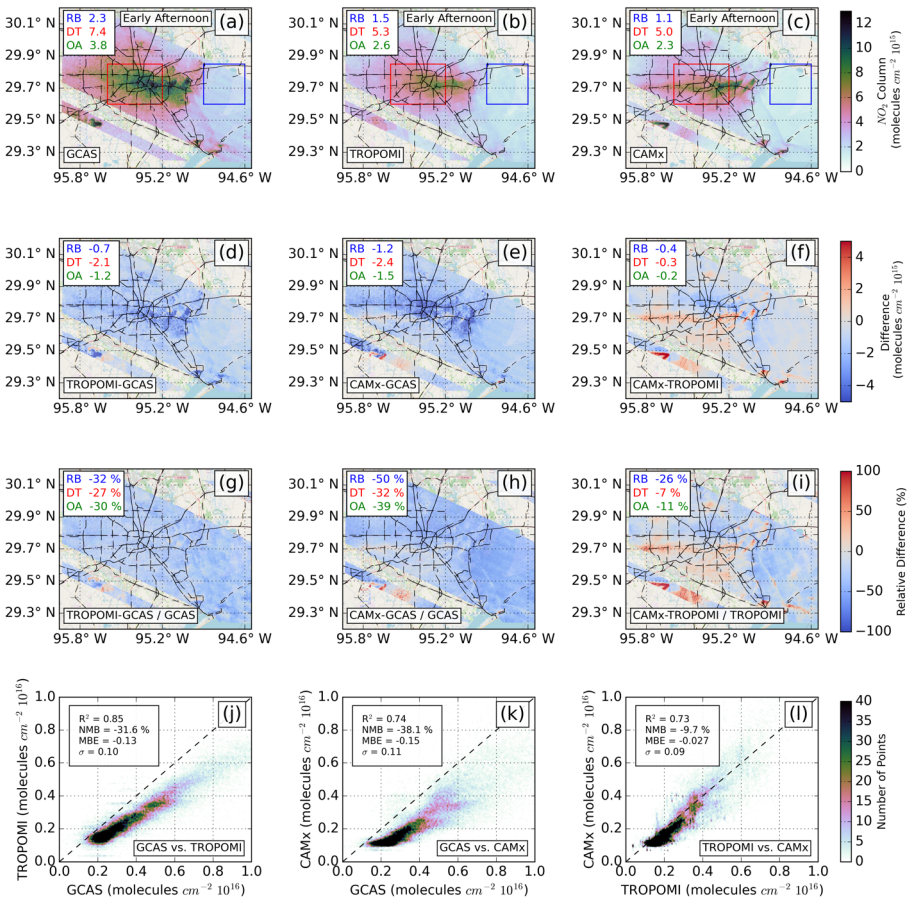

Figure 5: Spatial distribution of GCAS (A), TROPOMI (B), and CAMx (C) NO_2 columns averaged across the ten GCAS flight days when within 90 minutes of each TROPOMI overpass representing early afternoon NO_2 columns. We identify three distinct areas: downtown or "DT" (red), the low emissions East Galveston Bay or "RB" (blue), and all other areas or "OA" (green) and calculate the averages in the top left of each chart. Absolute differences between GCAS and TROPOMI (D), GCAS and CAMx (E), and TROPOMI and CAMx (F). Relative differences between GCAS and TROPOMI (G), GCAS and CAMx (H), and TROPOMI and CAMx (I). Scatter density plots of GCAS vs. TROPOMI (J), GCAS vs. CAMx (K), and TROPOMI vs. CAMx (L). © OpenStreetMap contributors 2023. Distributed under the Open Data Commons Open Database License (ODbL) v1.0.

First, we consider the spatial distribution of NO_2 columns from GCAS (Fig. 5A), TROPOMI (Fig. 5B), and CAMx (Fig. 5C) independently. For all three datasets, NO_2 columns are higher in downtown Houston than in the rural East Galveston Bay; generally, they are between 3 and 5 times as large. The two finer-resolution datasets – GCAS and CAMx – also capture NO_2 peaks associated with point sources like those from W A Parish, Texas City, and Baytown and in the Ship Channel. A map of the major point sources discussed in this work is included in the supplemental (Fig. S24). The coarser resolution of TROPOMI leads to fewer identifiable peaks associated with point sources; however, there are slightly elevated observed values near the W A Parish and Texas City power plants and the Ship Channel. Observations from GCAS and TROPOMI reveal a more diffuse peak in NO_2 columns in and around downtown Houston that includes elevated levels of NO_2 in the western part of the city. Simulated columns from CAMx, on the other hand, primarily estimate higher NO_2 values in the eastern area of downtown Houston and have lower NO_2 values in the western area of the city.

We next consider the three products compared to one another through three methods: absolute difference (Fig. 5D-F), relative difference (Fig. 5G-I), and scatter density plots (Fig. 5J-L). We intercompare these three products by isolating three sets of pairs: that is GCAS and TROPOMI, GCAS and CAMx, and TROPOMI and CAMx.

First, considering GCAS and TROPOMI, there appears to be a systematic low bias in TROPOMI observations throughout nearly the entire domain. Regardless of the spatial subset, the low bias in TROPOMI was consistent and ranged from -27% in downtown to -32% in the rural bay (Fig. 5G). In an absolute sense, on average TROPOMI was between 2.1 and 0.7 molecules cm^{-2} 10^{15} lower than GCAS (Fig. 5D) across the three locations. Throughout the entire domain, observations from GCAS and TROPOMI were well correlated (r^2=0.85), but TROPOMI had an overall negative normalized mean bias of -31.6% (Fig. 5J). We note that this low bias is slightly greater than what we would expect from considering the biases of these products relative to Pandora measurements as we do in section 3.1; doing this we would expect TROPOMI to be low biased relative to GCAS by around 23%. This slight additional negative bias indicates that either the three Pandora sites are unable to capture the full extent of the negative TROPOMI bias and that TROPOMI may be lower biased outside of these sites (e.g., areas outside of downtown Houston) or that GCAS observations may be biased additionally high outside of these sites. Notably, there are a few areas surrounding point sources in the eastern area of downtown and around the W A Parish plant in which TROPOMI observes higher NO_2 columns than GCAS. This is likely attributable to the coarser resolution of TROPOMI that results in peaks of NO_2 to be spread into surrounding areas that are in the same TROPOMI grid cell.

Second, comparing GCAS to CAMx we again find a low bias relative to GCAS, albeit one with a higher degree of spatial variability. In the remote bay, CAMx simulated columns are lower than GCAS compared to elsewhere in the domain (-50%) (Figure 5H) while downtown and background levels are similarly biased at 32% and 39%, respectively. This lower bias in the low emission East Galveston Bay is indicative of an underestimation of background NO_2 columns in the CAMx simulation. Across these three regions the mean absolute differences range

Deleted: .5
Deleted: 1
Deleted: 2
Deleted: 3
Deleted: 16
Deleted: 0.3
Deleted: 1
Deleted: 2
Deleted: 3
Deleted: 7
Deleted: 39
Deleted: 29
Deleted: in a relative sense

from -2.4 to -1.2 molecules cm^{-2} 10^{15} (Figure 5E). Visually, the negative bias in CAMx appears to be stronger in downtown and to the west, east, and north-west of downtown and less to the south and south-west of downtown. Overall, GCAS and CAMx are well correlated (r^2=0.74) (Figure 5K); however, simulated columns from CAMx have a worse negative bias (NMB=-38.1%) against GCAS than what is captured at the Pandora sites of approximately -21%. Around some point sources CAMx columns are positively biased against GCAS observations. This high bias in CAMx is likely attributable to differences in wind speed and direction in the WRF simulation than in reality. These differences could contribute to NO_2 plumes being advected in incorrect directions.

Lastly, when comparing observed columns from TROPOMI to simulated columns from CAMx, biases have a great degree of spatial variability; however, in general CAMx is negatively biased. In a relative sense (Fig. 5I), the CAMx simulated columns are lowest compared to TROPOMI in the rural bay (-26%) and similar in downtown (-7%) and in other areas (-11%). There are a few areas where this pattern does not hold: both in the area southwest of downtown Houston and near point sources, CAMx is biased high compared to TROPOMI. These results indicate that simulated columns from CAMx are underestimated in downtown Houston and that this underestimation could potentially be attributable to an incorrect advection of NO_2 from some downtown source to the south-west perhaps in conjunction with an underestimate of emissions in this downtown area. Overall, TROPOMI and CAMx are well correlated (r^2=0.73) and there is a spatially heterogeneous low bias when considering the two products throughout the domain (NMB = -9.7%) (Fig. 5L).

3.4 Comparisons of GCAS, TROPOMI, and CAMx data at a coarser resolution

The comparisons presented in the prior section are done at the high resolution of the CAMx grid (444 × 444 m^2). Here, we characterize the effect of the coarser resolution of TROPOMI by performing an additional comparison of the three datasets at the 0.05° × 0.05° resolution (approximately 5.5 × 5.5 km^2) (Fig. 6). We average all of the NO_2 columns from this finer resolution to the coarser resolution based on the centroid of the fine resolution grid cells. This new coarser resolution is comparable to that of the TROPOMI observations at nadir (on average 3.5 × 5.5 km^2). We additionally present comparisons at two further coarser resolutions in the supplemental: 0.25° × 0.25° (Fig. S25) and 0.1° × 0.1° (Fig. S26).

Deleted: 0.8
Deleted: 2
Deleted: 0
Deleted: 1
Deleted: 0
Deleted: 6
Deleted: 11
Deleted: the background
Deleted: 7
Formatted: Heading 1
Deleted: ¶
Deleted: 1
Deleted: 3
Deleted: 1
Deleted: 4

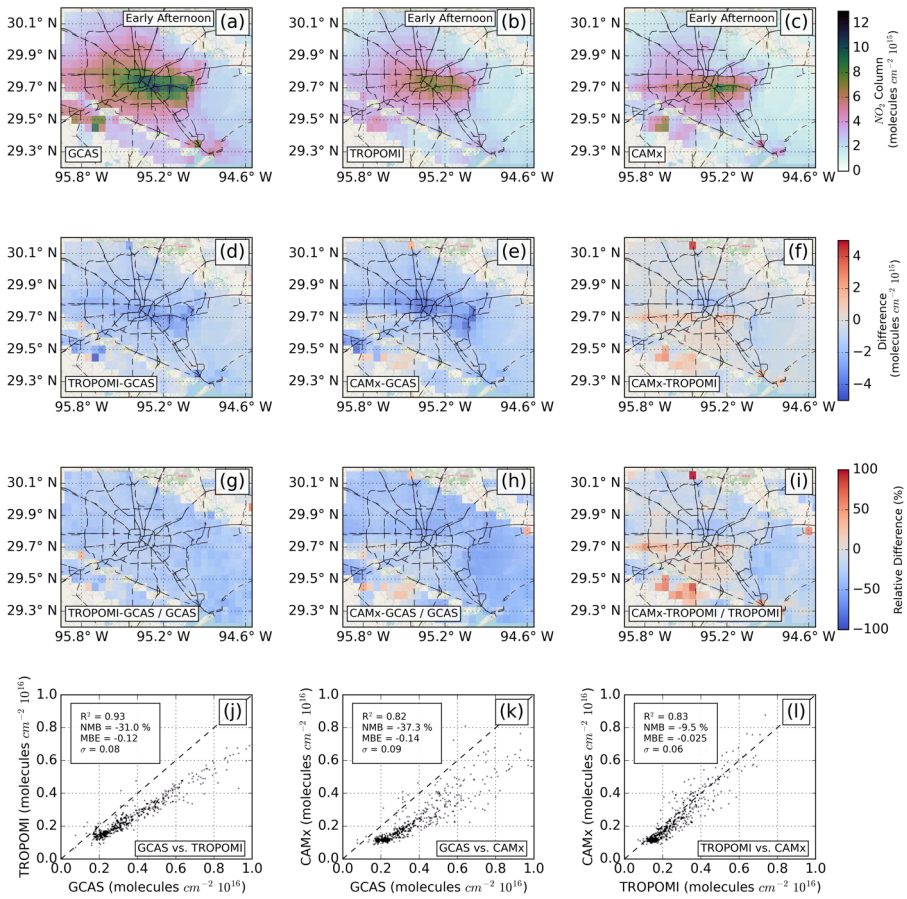

Figure 6: Spatial distribution of GCAS (A), TROPOMI (B), and CAMx (C) at the 0.05° × 0.05° resolution averaged across the ten GCAS flight days when within 1.5 hours of each TROPOMI overpass representing early afternoon NO_2 columns. Absolute differences between GCAS and TROPOMI (D), GCAS and CAMx (E), and TROPOMI and CAMx (F). Relative differences between GCAS and TROPOMI (G), GCAS and CAMx (E), and TROPOMI and CAMx (F). Scatter density plots of GCAS vs. TROPOMI (G), GCAS vs.

CAMx (H), and TROPOMI vs. CAMx (I). © OpenStreetMap contributors *2023*. Distributed under the Open Data Commons Open Database License (ODbL) v1.0.

Generally, this change in resolution has only a minor effect on the trends discussed in the prior section. Observed NO_2 columns from GCAS and TROPOMI have a collocated peak in downtown Houston and NO_2 columns from TROPOMI are still systematically biased lower compared to GCAS. Simulated NO_2 columns from CAMx are clearly lower than GCAS in the area directly west of downtown and slightly higher southwest of downtown compared to TROPOMI (Fig. 6A-C). Considering the spatial distribution of absolute (Fig. 6D-F) and relative (Fig. 6G-I) differences between the three products, the low bias in TROPOMI compared to GCAS is generally homogenous throughout the domain. On the other hand, there are clear peaks in negative biases in downtown and western Houston when comparing CAMx to GCAS and in some areas southwest of downtown biases are small and positive. Averaging observations to this coarser resolution improved the correlation for all three pairs (r^2=0.93, 0.82, and 0.83 for GCAS and TROPOMI, GCAS and CAMx, and TROPOMI and CAMx, respectively) while the biases remained comparable to what was found in the comparison at a finer resolution (Fig. 5J-L).

3.5 Weekend vs. weekday patterns across the datasets

Three of the ten GCAS flight days occurred on weekends (September 11th, 25th, and 26th) and observations from GCAS and TROPOMI – along with simulated NO_2 columns from CAMx –exhibited different patterns on weekends versus on weekdays (September 1st, 3rd, 8-10th, 23rd, 24th). This difference in observed and simulated patterns is explored in greater detail in this section, first through comparisons to Pandora measurements (Fig. 7) and then through spatial comparisons of the products on weekdays versus on weekends (Fig. 8). When interpreting these results, it should be considered that weekend data is limited to only three days. This data sparsity introduces a high degree of uncertainty in conclusions derived from this analysis. Day to day changes in meteorological conditions are likely responsible for some of the exhibited differences so they cannot solely be attributed to differences in emission patterns.

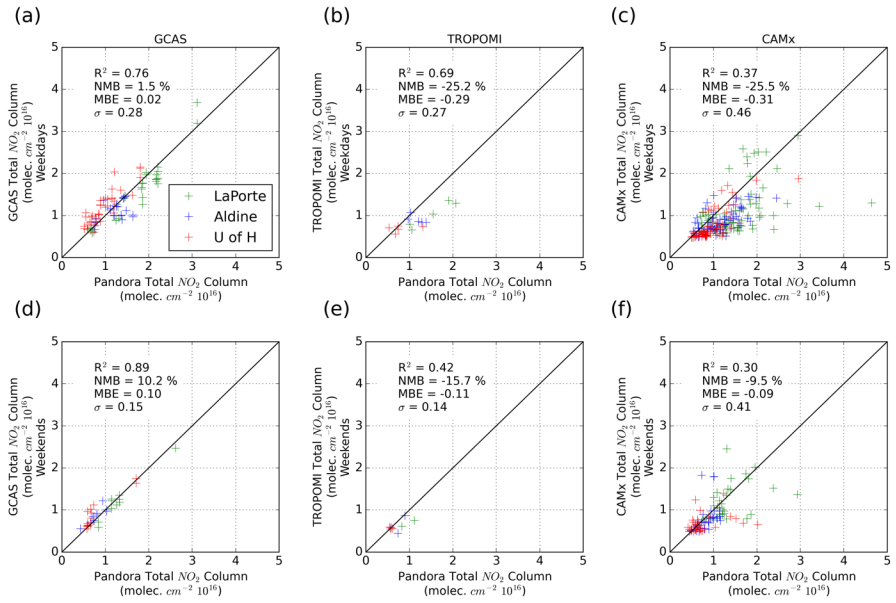

Figure 7: Comparison of GCAS (A), TROPOMI (B), and CAMx (C) to Pandora on weekdays and of GCAS (D), TROPOMI (E), and CAMx (F) to Pandora on weekends. Data from all possible overpasses coincident within 15 minutes of a Pandora observation are considered. GCAS flight times generally ranged from 8:00 AM-4:00 PM CDT. TROPOMI overpasses occurred around 1:30 PM local time.

First, we consider how comparisons of the observational datasets – GCAS and TROPOMI – with Pandora change on weekends compared to weekdays. Biases for both GCAS and TROPOMI become more positive on weekends, NMB=10.2% and NMB=-15.7%, respectively, than on weekdays, NMB=1.5% and NMB=-25.2%. GCAS observations are slightly better correlated to Pandora measurements on weekends (r^2=0.89 versus r^2=0.76); however, TROPOMI observations are worse correlated (r^2=0.42 versus r^2=0.69) that is likely attributable to a limited number of observations that are at lower NO_2 column levels with limited dynamic range. Overall, biases are slightly worse for GCAS and better for TROPOMI on weekends; however, given the small number of measurements it is unclear whether this pattern is attributable to meteorological conditions or if it is attributable to some systematic bias in the instruments.

Simulated NO_2 columns from CAMx exhibit clearer weekday versus weekend patterns, and since these simulated columns are available for every hour of the day there is a greater number of measurements to support these findings

Deleted: 4

Deleted: 1

Deleted: -1

Deleted: 0

than for the two observational datasets. While the correlation is slightly degraded on weekends (r^2=0.30 versus r^2=0.37) the negative bias in simulated columns compared to Pandora measurements is reduced on weekends (NMB=-25.5% versus NMB=-9.5%).

Deleted: 1
Deleted: 7
Deleted: 9
Deleted: 7
Deleted: 14
Deleted: 2

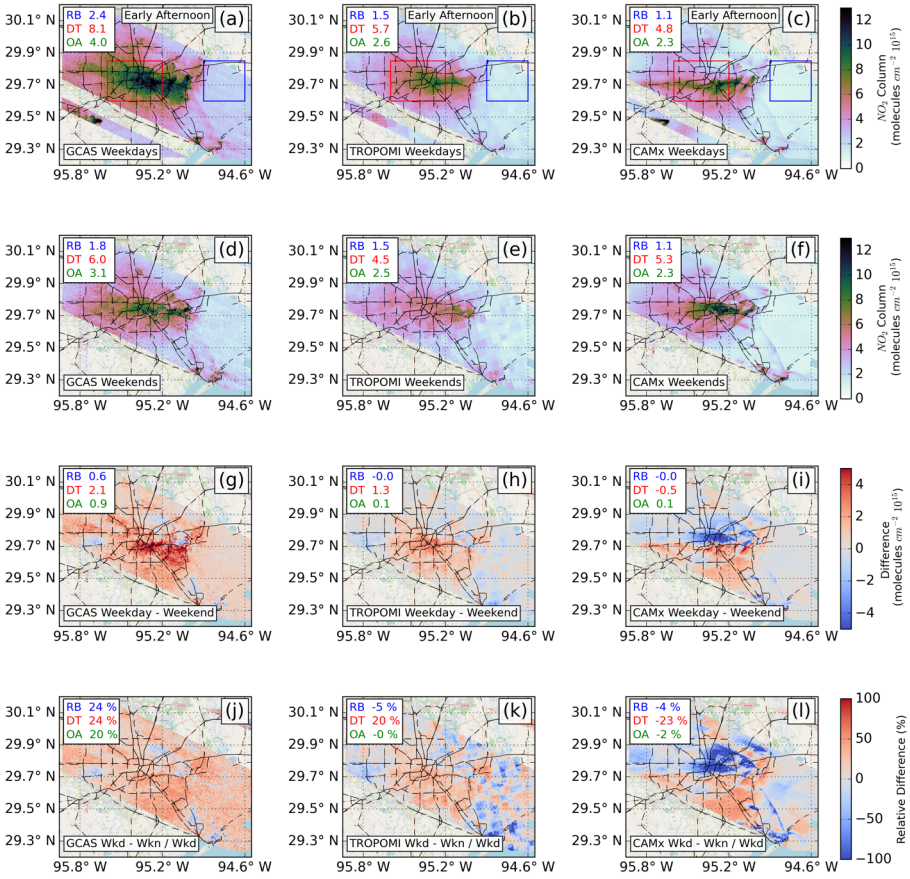

Figure. 8: Spatial Distribution of GCAS, TROPOMI, and CAMx NO_2 columns on weekdays (A-C), weekends (D-F), and the absolute difference between weekdays and weekends (G-I) and relative difference (J-L). Data are averaged across the GCAS flight days corresponding to weekdays or weekends when within 1.5 hours of each TROPOMI overpass representing early afternoon NO_2 columns. We identify three distinct areas: downtown or "DT" (red), the low emissions East Galveston Bay or "RB" (blue), and all other areas or "OA" (green) and calculate the averages in the top left of each chart. © OpenStreetMap contributors 2023. Distributed under the Open Data Commons Open Database License (ODbL) v1.0.

GCAS and TROPOMI observations of NO_2 column concentrations are higher on weekdays (Fig. 8A, B) than on weekends (Fig. 8D, E). This is true in downtown Houston and the rural bay where weekday GCAS observations are 2.1 molecules cm^{-2} 10^{15} (24%) and 0.6 molecules cm^{-2} 10^{15} (24%) higher, respectively, on weekdays than on weekends. In other areas of Houston, GCAS observations on weekdays are higher than weekends but not to the same degree (20%). A similar pattern occurs for TROPOMI, in downtown Houston TROPOMI columns are 20% higher on weekdays than on weekends but comparable in other areas and -5% lower in the rural bay. This comparison again implicates some underestimated weekday source of NO_2 in CAMx that is of great importance in the western area of Houston; however, due to the lack of data on weekends – that is apparent in the discontinuities in the weekend NO_2 column concentrations of TROPOMI – it is difficult to examine this quantitatively.

Comparing weekday columns simulated from CAMx with weekend columns, we find that the mean concentrations for the three defined areas are nearly identical (Fig. 8C and F), although columns on weekdays are higher south and southwest of downtown while columns on weekends are higher within downtown. These spatial patterns are further revealed in the difference plots (Fig. 8I and 8L) where the difference in weekday versus weekend values appear to be split right along I-10; north of I-10 weekday values are much lower than weekend values while south of I-10 the opposite is true. This difference is likely attributable to different meteorological conditions on these days. Overall, simulated CAMx columns are substantially lower than GCAS and TROPOMI on weekdays but more similar on weekends implying that weekday emissions may be underestimated in the TCEQ inventory.

Deleted: 6

Deleted: 8

Deleted: 19

3.6 Relevance to TEMPO: Diurnal patterns in column and surface NO_2

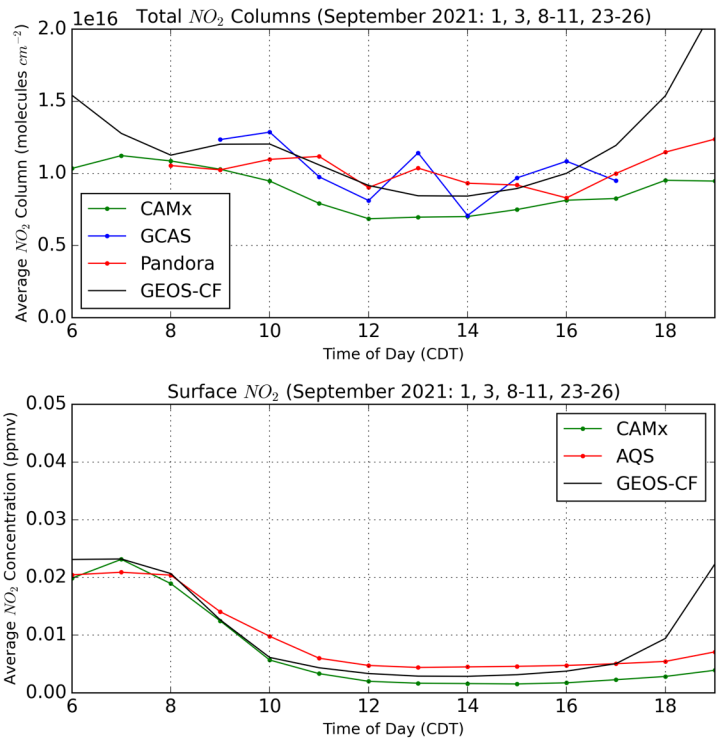

Figure 9: Diurnal patterns in Total NO_2 columns (top) averaged across the three Pandora sites and 10 flight days from CAMx (green), GCAS (blue), Pandora (red), and GEOS-CF (black). Diurnal patterns in surface-level NO_2 concentrations (bottom) in downtown Houston for CAMx and GEOS-CF averaged across the 10 flight days and across all monitors in Harris County for AQS surface-level monitors (red).

Lastly, we characterize the diurnal profiles of simulated and observed NO_2 columns during the TRACER-AQ campaign in downtown Houston (Fig. 9). First, considering column concentrations, we find generally good agreement during the early morning (8:00 -10:00 local time) across the two simulated datasets (CAMx and GEOS-CF) and two observational datasets (GCAS and Pandora). Interestingly, between 9:00 and 11:00 local time, Pandora column measurements show a slight increase, while model simulations show a slight decrease during the same time

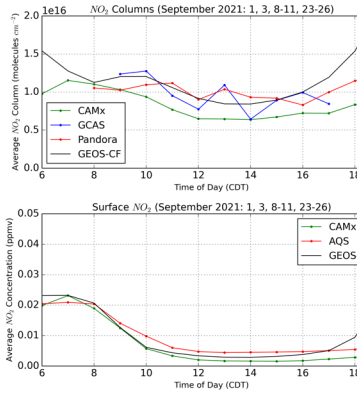

Deleted:

Deleted: late

Deleted: am

Deleted: am

interval. During midday and the afternoon (11:00 – 16:00 local time) – that corresponds to the period with the most GCAS observations – GEOS-CF columns generally agree well with Pandora observations. In the evening (17:00 – 19:00 local time), GEOS-CF columns have a substantial high bias across these flight days. The GEOS-CF mismatch in the evening has implications for TEMPO NO_2 evening retrievals if this is a persistent bias in other urban areas since satellite instruments are especially sensitive to *a priori* assumptions at low sun angles.

Second, considering surface concentrations, we see a similar trend. Generally, there is great agreement across the three datasets (CAMx, AQS observations, and GEOS-CF) in the early morning (6:00 – 9:00 local time) before they begin to diverge with the two simulated produces maintaining comparable magnitudes with low biases compared to surface monitors. At around midday to the afternoon (12:00 – 17:00 local time) both simulated products have a low bias compared to observed surface-level NO_2; however, the bias in CAMx concentrations is worse. Some of the apparent low bias may be related to an artificial high bias in NO_2 chemiluminescence surface monitors (Dunlea et al., 2007; Lamsal et al., 2008). In the evening (18:00 – 19:00 local time), surface-level NO_2 from GEOS-CF climbs rapidly; however, observed NO_2 from the AQS and simulated NO_2 from CAMx increase only slightly. The large increase in NO_2 in GEOS-CF in the evening appears at both the surface and in the column potentially indicating issues capturing boundary layer dynamics.

4 Conclusions

This study leveraged observational datasets of NO_2 column densities from three instruments – Pandora ground-based spectrometers, the airborne GCAS instrument, and the satellite TROPOMI instrument. These instruments were used to investigate NO_2 column densities in Houston, TX during the September 2021 TRACER-AQ campaign and to characterize strengths/weaknesses and uncertainties in the respective datasets. These observational datasets were then compared to simulated NO_2 columns from CAMx to characterize the performance of the simulation and to identify potential under- or overestimates of emissions in the simulation. We find that GCAS has strong agreement with Pandora instruments (r^2=0.79 and NMB=3.4%) during its overpasses and that TROPOMI also has strong performance but an important low bias – consistent with validation by the European Space Agency (Verhoelst et al., 2021) – across the urban Houston locations (r^2=0.73 and NMB=-22.8%). This low bias in TROPOMI observations persists despite the inclusion of an air mass factor derived from the CAMx simulation. When comparing different versions of TROPOMI we find differences between the v2.3.1, v2.4.0, and NASA MINDS product and find that the MINDS (r^2=0.69 and NMB=-18.2%) and version 2.3.1 (r^2=0.72 and NMB=-18.3%) products – with the CAMx AMF – performs comparably and both outperform version 2.4.0 considering bias albeit with slightly worse correlation. The performance of the CAMx simulation varied depending on the day, but overall, simulated NO_2 columns were more poorly correlated and more negatively biased compared to Pandora measurements than the observational datasets (r^2=0.34 and NMB= -21.2%). Notably, this low bias in CAMx simulated NO_2 columns improved on weekends (NMB=-9.5%) – albeit over a limited number of days. This improvement on weekends implicates that a source that emits in greater amounts on weekdays (e.g., heavy-duty vehicles) could be

Deleted: 11 am-4 pm
Deleted: 5pm
Deleted: -
Deleted: 7pm
Formatted: Font: Italic
Deleted: While CAMx is low biased throughout most of the day it maintains the same magnitude of change as Pandora reflecting a similar temporal pattern.
Deleted: am-
Deleted: am
Deleted: pm-
Deleted: 5 pm
Field Code Changed
Deleted: 6 pm-7 pm
Deleted: stably
Deleted: is
Deleted: in GEOS-CF
Deleted: a consistent high bias as the
Deleted: height decreases which is perhaps attributable to its coarser horizontal and vertical resolution
Deleted: Overall, simulated surface concentrations and column concentrations from CAMx appear to perform at their worst during the late morning and afternoon compared to observations from Pandora, GCAS, and AQS monitors and there is greater agreement in the early morning and evening.…
Deleted: 80
Deleted: 0
Deleted: 1
Field Code Changed
Deleted: but
Deleted: 4
Deleted: 5
Deleted: 5
Deleted: 14
Deleted: 2

underestimated in the TCEQ inventory; however, we cannot say this conclusively given the limited number of observations on weekends. The poor correlation in the simulated NO_2 columns is likely attributable to minor wind directional errors – simulated wind direction had a MAE that ranged from 14° to 32° when compared to observations – and spatial correlations over larger extents match well.

When we compare the spatial distribution of TROPOMI observations to GCAS (Fig. 3 and 4) we find that the low bias in TROPOMI NO_2 columns is perhaps stronger than the low bias implied at the three Pandora sites – this could be a resolution constraint of the coarser TROPOMI product that is unable to capture the fine-scale features in NO_2 column concentrations that GCAS is able to. If coarse resolution is responsible for this low-bias, new instruments on geostationary satellites from missions like the NASA TEMPO mission could be leveraged to further improve satellite-derived estimates of urban NO_2 in cities like Houston. CAMx comparisons to GCAS, when extended beyond the limited number of Pandora sites, indicate that the CAMx simulated low bias could be substantially worse than at the Pandora sites (-32%) in downtown and west of downtown Houston. This overall underestimate in the CAMx simulations is potentially attributable to a number of confounding factors including an inability of the WRF simulation to capture local meteorology and an underestimate of emissions in sectors that are more spatially located in downtown and western Houston like on-road mobile emissions. We also consider differences in the diurnal profiles of surface and column NO_2 across multiple datasets and find that the performance of CAMx is at its worst in the late morning and early afternoon and performance is better during other times of the day.

There is a clear negative bias in the CAMx simulated NO_2 columns compared to GCAS observations. Although we evaluate the performance of WRF at the surface, we do not consider vertical advection and the vertical mixing scheme in WRF merits further investigation. A previous study by Liu et al., (2023) has investigated this for the TRACER-AQ campaign in Houston, albeit with a different chemical transport model, and found generally good agreement in potential temperature but an underestimate of ozone in the free troposphere. Given the worse performance of WRF-CAMx at the surface (NMB=-59%) than for the columns (-22%), if the vertical mixing scheme has poor performance we suspect it to be due to overmixing leading to the rapid removal of surface-level NO_2. Additionally, the low bias in the TROPOMI observations compared to Pandora and GCAS merits further investigation; the role of algorithm and resolution could be considered by comparing different versions and finer-resolution geostationary observations in the future beyond what is considered in this study. The reference background NO_2 from TROPOMI used in GCAS could also introduce error into these results that should be considered. Given the fine resolution of GCAS observations and CAMx simulated column concentrations there is potential for investigations into how air pollution is inequitably distributed across different populations in Houston and how specific sources contribute to these inequities. The findings presented here imply that TROPOMI derived NO_2 column concentrations may be underestimated in Houston if not corrected for in applications such as exposure assessments, and NO_x emissions derivations.

This analysis benefitted from three independent measurement datasets (i.e., Pandora, TROPOMI, and GCAS) that were critical to isolate the negative biases in TROPOMI and CAMx although we note that negative biases in TROPOMI have been mentioned in earlier literature (e.g., Verhoelst et al, 2021) and in the quarterly issued operational

Deleted: a

Deleted: Tropospheric Emissions: Monitoring of Pollution (TEMPO)

Deleted: p

Deleted: 1.0

Deleted: ¶

Field Code Changed

Deleted: (

Deleted:

Deleted: x

Formatted: Font: Not Italic

Formatted: Space Before: Auto, After: Auto

validation reports (available at https://mpc-vdaf.tropomi.eu/). It is common to consider TROPOMI measurements as accurate representation of NO_2 column concentrations; however, if we had done so in this study, we would have failed to identify the substantial negative bias in the CAMx simulation of column concentrations. Observations from multiple Pandora instruments and GCAS overpasses made it possible to isolate negative biases in TROPOMI and CAMx. Lastly, given the relatively minimal biases in WRF simulated meteorology compared to observations, low NO_2 biases in the simulated CAMx column concentrations imply that current TCEQ NO_x emissions inventories in the Houston area used to drive the CAMx simulation may be underestimated, and that this underestimation is likely attributable to a source with weekday-weekend differences and correlated with roadways and/or population density.

Deleted: This analysis benefitted from three independent measurement datasets (i.e., Pandora, TROPOMI, and GCAS) that were critical to isolate the negative biases in TROPOMI and CAMx

Deleted: .

Deleted: low

Deleted:

Deleted: – and the relatively good agreement between WRF simulated meteorological conditions and observations –

Deleted:

Deleted: x

Deleted: substantial

Formatted: Font: Italic, English (UK)

Acknowledgements

The authors of this paper acknowledge Elena Lind, Alex Kotsakis, the NASA Pandora Project and LuftBlick for their contribution in deploying, operating, and processing data from the Pandora spectrometers during TRACER-AQ, the NASA Tropospheric Composition Program and the Texas Commission on Environmental Quality for TRACER-AQ support, and the TRACER-AQ science team for their useful contributions. We also acknowledge the use of Google Earth for the background map used in Fig. 1. The authors acknowledge the use of OpenStreetMaps for the background maps in Fig. 2, 4, 5, 6, 8 and S2-14. The authors also acknowledge funding from the NASA Atmospheric Composition Modelling and Analysis Program (ACMAP) (80NSSC23K1002). The preparation of this manuscript was funded by a grant from the Texas Air Quality Research Program (AQRP) at The University of Texas at Austin through the Texas Emission Reduction Program (TERP) and the Texas Commission on Environmental Quality (TCEQ). The findings, opinions and conclusions are the work of the authors and do not necessarily represent findings, opinions, or conclusions of the AQRP or the TCEQ. This work contains modified Copernicus Sentinel-5 Precursor data processed by KNMI and post-processed by George Washington University.

Deleted:

Code Availability

The scripts used to process these data for the intercomparison are available by correspondence with the authors upon reasonable request.

Data Availability

Ground level EPA AQS observations are available from EPA Air Data: https://www.epa.gov/outdoor-air-quality-data. GEOS-CF data are available from the GrADS data server: https://opendap.nccs.nasa.gov/dods/. TROPOMI NO_2 column data are publicly available from the Copernicus Data Space Ecosystem: https://dataspace.copernicus.eu. GCAS and CAMx data are publicly available via NASA's Atmospheric Sciences Data Center:

Field Code Changed

https://doi.org/10.5067/ASDC/SUBORBITAL/TRACERAQ/DATA001/GV/AircraftRemoteSensing/GCAS_1 as are Pandora data https://asdc.larc.nasa.gov/project/TRACER-AQ/TRACERAQ_Pandora_Data_1.

Field Code Changed

Author Contributions

D.G., developed the project design, J.J. and G.Y. set-up and conducted the WRF-CAMx simulations, L.J. and the TRACER-AQ science team measured and processed the GCAS and Pandora Data, D.G downloaded and processed the TROPOMI Data and regridded all data to the WRF-CAMx grid, M.O.N further processed the data to match temporally and spatially, conducted the intercomparison, wrote the manuscript, and generated the figures except Fig. 1 and Fig. S1 that were generated by J.J. and D.G., respectively, B.D. gave feedback on the methodology, all authors edited the manuscript and gave feedback on the figures.

Deleted: 4

Competing Interests

The authors declare that they have no conflict of interest.

References

Achakulwisut, P., Brauer, M., Hystad, P., & Anenberg, S. C. (2019). Global, national, and urban burdens of paediatric asthma incidence attributable to ambient NO2 pollution: Estimates from global datasets. *The Lancet Planetary Health*, *3*(4), e166–e178. https://doi.org/10.1016/S2542-5196(19)30046-4

Anenberg, S. C., Mohegh, A., Goldberg, D. L., Kerr, G. H., Brauer, M., Burkart, K., Hystad, P., Larkin, A., Wozniak, S., & Lamsal, L. (2022). Long-term trends in urban NO2 concentrations and associated paediatric asthma incidence: Estimates from global datasets. *The Lancet Planetary Health*, *6*(1), e49–e58. https://doi.org/10.1016/S2542-5196(21)00255-2

Boersma, K. F., Eskes, H. J., Richter, A., De Smedt, I., Lorente, A., Beirle, S., van Geffen, J. H. G. M., Zara, M., Peters, E., Van Roozendael, M., Wagner, T., Maasakkers, J. D., van der A, R. J., Nightingale, J., De Rudder, A., Irie, H., Pinardi, G., Lambert, J.-C., & Compernolle, S. C. (2018). Improving algorithms and uncertainty estimates for satellite NO_2 retrievals: Results from the quality assurance for the essential climate variables (QA4ECV) project. *Atmospheric Measurement Techniques*, *11*(12), 6651–6678. https://doi.org/10.5194/amt-11-6651-2018

Formatted: Font: (Default) Times New Roman

Bucsela, E. J., Krotkov, N. A., Celarier, E. A., Lamsal, L. N., Swartz, W. H., Bhartia, P. K., Boersma, K. F., Veefkind, J. P., Gleason, J. F., & Pickering, K. E. (2013). A new stratospheric and tropospheric NO_2 retrieval algorithm for nadir-viewing satellite instruments: Applications to OMI. *Atmospheric Measurement Techniques*, *6*(10), 2607–2626. https://doi.org/10.5194/amt-6-2607-2013

Cede, A. (2021). *Manual for Blick Software Suite 1.8*.

Collaboration, T. A., Price-Whelan, A. M., Lim, P. L., Earl, N., Starkman, N., Bradley, L., Shupe, D. L., Patil, A. A., Corrales, L., Brasseur, C. E., Nöthe, M., Donath, A., Tollerud, E., Morris, B. M., Ginsburg, A., Vaher, E., Weaver, B. A., Tocknell, J., Jamieson, W., … Contributors, A. P. (2022). The Astropy Project: Sustaining and Growing a Community-oriented Open-source Project and the Latest Major Release (v5.0) of the Core Package*. *The Astrophysical Journal*, *935*(2), 167. https://doi.org/10.3847/1538-4357/ac7c74

Danckaert, T., Fayt, C., Roozendael, M. V., Smedt, I. D., Letocart, V., Merlaud, A., & Pinardi, G. (2017). *QDOAS Software user manual*.

de Foy, B., Lei, W., Zavala, M., Volkamer, R., Samuelsson, J., Mellqvist, J., Galle, B., Martínez, A.-P., Grutter, M., Retama, A., & Molina, L. T. (2007). Modelling constraints on the emission inventory and on vertical dispersion for CO and SO_2 in the Mexico City Metropolitan Area using Solar FTIR and zenith sky UV spectroscopy. *Atmospheric Chemistry and Physics*, *7*(3), 781–801. https://doi.org/10.5194/acp-7-781-2007

de Foy, B., Wilkins, J. L., Lu, Z., Streets, D. G., & Duncan, B. N. (2014). Model evaluation of methods for estimating surface emissions and chemical lifetimes from satellite data. *Atmospheric Environment*, *98*, 66–77. https://doi.org/10.1016/j.atmosenv.2014.08.051

Demetillo, M. A. G., Navarro, A., Knowles, K. K., Fields, K. P., Geddes, J. A., Nowlan, C. R., Janz, S. J., Judd, L. M., Al-Saadi, J., Sun, K., McDonald, B. C., Diskin, G. S., & Pusede, S. E. (2020). Observing Nitrogen Dioxide Air Pollution Inequality Using High-Spatial-Resolution Remote Sensing Measurements in Houston, Texas. *Environmental Science & Technology*, *54*(16), 9882–9895. https://doi.org/10.1021/acs.est.0c01864

DOC/NOAA/NWS/NCEP/EMC. (2023). *Global Data Assimilation System (GDAS)* [dataset]. https://www.ncei.noaa.gov/access/metadata/landing-page.

Dunlea, E. J., Herndon, S. C., Nelson, D. D., Volkamer, R. M., Martini, F. S., Sheehy, P. M., Zahniser, M. S., Shorter, J. H., Wormhoudt, J. C., Lamb, B. K., Allwine, E. J., Gaffney, J. S., Marley, N. A., Grutter, M.,

Marquez, C., Blanco, S., Cardenas, B., Retama, A., Villegas, C. R. R., … Molina, M. J. (2007). Evaluation of nitrogen dioxide chemiluminescence monitors in a polluted urban environment. *Atmos. Chem. Phys.*, 14.

EPA. (2023). *United States Environmental Protection Agency (EPA). "Clean Air Markets Program Data." Washington, DC: Office of Atmospheric Protection, Clean Air Markets Division. Available from EPA's Air Markets Program Data web site: Https://campd.epa.gov/.* [dataset]. https://campd.epa.gov/.

Eskes, H. J., Eichmann, K.-U., Lambert, J.-C., Loyola, D., Stein-Zweers, D., Dehn, A., & Zehner, C. (2023). *S5P MPC Product Readme Nitrogen Dioxide*.

European Space Agency. (2021). *Copernicus Sentinel-5P TROPOMI* [dataset]. European Space Agency. https://doi.org/10.5270/S5P-9bnp8q8

Ge, S., Wang, S., Xu, Q., & Ho, T. (2021). Source apportionment simulations of ground-level ozone in Southeast Texas employing OSAT/APCA in CAMx. *Atmospheric Environment*, *253*, 118370. https://doi.org/10.1016/j.atmosenv.2021.118370

Geddes, J. A., Martin, R. V., Bucsela, E. J., McLinden, C. A., & Cunningham, D. J. M. (2018). Stratosphere–troposphere separation of nitrogen dioxide columns from the TEMPO geostationary satellite instrument. *Atmospheric Measurement Techniques*, *11*(11), 6271–6287. https://doi.org/10.5194/amt-11-6271-2018

Goldberg, D. L., Harkey, M., de Foy, B., Judd, L., Johnson, J., Yarwood, G., & Holloway, T. (2022). Evaluating NO_x emissions and their effect on O_3 production in Texas using TROPOMI NO_2 and HCHO. *Atmospheric Chemistry and Physics*, *22*(16), 10875–10900. https://doi.org/10.5194/acp-22-10875-2022

Guenther, A. B., Jiang, X., Heald, C. L., Sakulyanontvittaya, T., Duhl, T., Emmons, L. K., & Wang, X. (2012). The Model of Emissions of Gases and Aerosols from Nature version 2.1 (MEGAN2.1): An extended and updated framework for modeling biogenic emissions. *Geoscientific Model Development*, *5*(6), 1471–1492. https://doi.org/10.5194/gmd-5-1471-2012

Herman, J., Cede, A., Spinei, E., Mount, G., Tzortziou, M., & Abuhassan, N. (2009). NO2 column amounts from ground-based Pandora and MFDOAS spectrometers using the direct-sun DOAS technique: Intercomparisons and application to OMI validation. *Journal of Geophysical Research: Atmospheres*, *114*(D13). https://doi.org/10.1029/2009JD011848

Huang, S., Li, H., Wang, M., Qian, Y., Steenland, K., Caudle, W. M., Liu, Y., Sarnat, J., Papatheodorou, S., & Shi, L. (2021). Long-term exposure to nitrogen dioxide and mortality: A systematic review and meta-analysis. *The Science of the Total Environment*, *776*, 145968. https://doi.org/10.1016/j.scitotenv.2021.145968

Hudman, R. C., Moore, N. E., Mebust, A. K., Martin, R. V., Russell, A. R., Valin, L. C., & Cohen, R. C. (2012). Steps towards a mechanistic model of global soil nitric oxide emissions: Implementation and space based-constraints. *Atmospheric Chemistry and Physics*, *12*(16), 7779–7795. https://doi.org/10.5194/acp-12-7779-2012

Jia, J., Cheng, S., Liu, L., Lang, J., Wang, G., Chen, G., & Liu, X. (2017). An Integrated WRF-CAMx Modeling Approach for Impact Analysis of Implementing the Emergency PM2.5 Control Measures during Red Alerts in Beijing in December 2015. *Aerosol and Air Quality Research*, *17*(10), 2491–2508. https://doi.org/10.4209/aaqr.2017.01.0009

Jin, X., Zhu, Q., & Cohen, R. C. (2021). Direct estimates of biomass burning NO_x emissions and lifetimes using daily observations from TROPOMI. *Atmospheric Chemistry and Physics*, *21*(20), 15569–15587. https://doi.org/10.5194/acp-21-15569-2021

Judd, L. M., Al-Saadi, J. A., Szykman, J. J., Valin, L. C., Janz, S. J., Kowalewski, M. G., Eskes, H. J., Veefkind, J. P., Cede, A., Mueller, M., Gebetsberger, M., Swap, R., Pierce, R. B., Nowlan, C. R., Abad, G. G., Nehrir, A., & Williams, D. (2020). Evaluating Sentinel-5P TROPOMI tropospheric NO_2 column densities with airborne and Pandora spectrometers near New York City and Long Island Sound. *Atmospheric Measurement Techniques*, *13*(11), 6113–6140. https://doi.org/10.5194/amt-13-6113-2020

Judd, L. M., Sullivan, J. T., Lefer, B., Haynes, J., Jensen, M. P., & Nadkarni, R. (2021). *TRACER-AQ Science Plan*.

Keller, C. A., Knowland, K. E., Duncan, B. N., Liu, J., Anderson, D. C., Das, S., Lucchesi, R. A., Lundgren, E. W., Nicely, J. M., Nielsen, E., Ott, L. E., Saunders, E., Strode, S. A., Wales, P. A., Jacob, D. J., & Pawson, S. (2021). Description of the NASA GEOS Composition Forecast Modeling System GEOS-CF v1.0. *Journal of Advances in Modeling Earth Systems*, *13*(4), e2020MS002413. https://doi.org/10.1029/2020MS002413

Kim, S.-W., McKeen, S. A., Frost, G. J., Lee, S.-H., Trainer, M., Richter, A., Angevine, W. M., Atlas, E., Bianco, L., Boersma, K. F., Brioude, J., Burrows, J. P., de Gouw, J., Fried, A., Gleason, J., Hilboll, A., Mellqvist, J., Peischl, J., Richter, D., … Williams, E. (2011). Evaluations of NO_x and highly reactive VOC emission inventories in Texas and their implications for ozone plume simulations during the Texas Air Quality Study

2006. *Atmospheric Chemistry and Physics*, *11*(22), 11361–11386. https://doi.org/10.5194/acp-11-11361-2011

Kowalewski, M. G., & Janz, S. J. (2014). Remote sensing capabilities of the GeoCAPE Airborne Simulator. *Earth Observing Systems XIX*, *9218*, 496–507. https://doi.org/10.1117/12.2062058

Lambert, J.-C., Claas, J., Stein-Zweers, D., Ludewig, A., Loyola, D., Sneep, M., & Dehn, A. (2023). *Quarterly Validation Report of the Copernicus Sentinel-5 Precursor Operational Data Products #19*.

Lamsal, L. N., Krotkov, N. A., Marchenko, S. V., Joiner, J., Oman, L., Vasilkov, A., Fisher, B., Qin, W., Yang, E.-S., Fasnacht, Z., Choi, S., Leonard, P., & Haffner, D. (2022). *TROPOMI/S5P NO2 Tropospheric, Stratospheric and Total Columns MINDS 1-Orbit L2 Swath 5.5 km x 3.5 km, NASA Goddard Space Flight Center, Goddard Earth Sciences Data and Information Services Center*.

Lamsal, L. N., Martin, R. V., van Donkelaar, A., Steinbacher, M., Celarier, E. A., Bucsela, E., Dunlea, E. J., & Pinto, J. P. (2008). Ground-level nitrogen dioxide concentrations inferred from the satellite-borne Ozone Monitoring Instrument. *Journal of Geophysical Research: Atmospheres*, *113*(D16). https://doi.org/10.1029/2007JD009235

Leitch, J. W., Delker, T., Good, W., Ruppert, L., Murcray, F., Chance, K., Liu, X., Nowlan, C., Janz, S. J., Krotkov, N. A., Pickering, K. E., Kowalewski, M., & Wang, J. (2014). The GeoTASO airborne spectrometer project. *Earth Observing Systems XIX*, *9218*, 487–495. https://doi.org/10.1117/12.2063763

Li, K.-F., Khoury, R., Pongetti, T. J., Sander, S. P., Mills, F. P., & Yung, Y. L. (2021). Diurnal variability of stratospheric column NO_2 measured using direct solar and lunar spectra over Table Mountain, California (34.38° N). *Atmospheric Measurement Techniques*, *14*(12), 7495–7510. https://doi.org/10.5194/amt-14-7495-2021

Li, W., Wang, Y., Liu, X., Soleimanian, E., Griggs, T., Flynn, J., & Walter, P. (2023). Understanding offshore high-ozone events during TRACER-AQ 2021 in Houston: Insights from WRF-CAMx photochemical modeling. *EGUsphere*, 1–21. https://doi.org/10.5194/egusphere-2023-1117

Liu, X., Wang, Y., Wasti, S., Li, W., Soleimanian, E., Flynn, J., Griggs, T., Alvarez, S., Sullivan, J. T., Roots, M., Twigg, L., Gronoff, G., Berkoff, T., Walter, P., Estes, M., Hair, J. W., Shingler, T., Scarino, A. J., Fenn, M., & Judd, L. (2023). Evaluating WRF-GC v2.0 predictions of boundary layer height and vertical ozone

profile during the 2021 TRACER-AQ campaign in Houston, Texas. *Geoscientific Model Development*, *16*(18), 5493–5514. https://doi.org/10.5194/gmd-16-5493-2023

Lorente, A., Boersma, K. F., Eskes, H. J., Veefkind, J. P., van Geffen, J. H. G. M., de Zeeuw, M. B., Denier van der Gon, H. a. C., Beirle, S., & Krol, M. C. (2019). Quantification of nitrogen oxides emissions from build-up of pollution over Paris with TROPOMI. *Scientific Reports*, *9*(1), Article 1. https://doi.org/10.1038/s41598-019-56428-5

Luke, W. T., Kelley, P., Lefer, B. L., Flynn, J., Rappenglück, B., Leuchner, M., Dibb, J. E., Ziemba, L. D., Anderson, C. H., & Buhr, M. (2010). Measurements of primary trace gases and NOY composition in Houston, Texas. *Atmospheric Environment*, *44*(33), 4068–4080. https://doi.org/10.1016/j.atmosenv.2009.08.014

Mazzuca, G. M., Ren, X., Loughner, C. P., Estes, M., Crawford, J. H., Pickering, K. E., Weinheimer, A. J., & Dickerson, R. R. (2016). Ozone production and its sensitivity to NO_x and VOCs: Results from the DISCOVER-AQ field experiment, Houston 2013. *Atmospheric Chemistry and Physics*, *16*(22), 14463–14474. https://doi.org/10.5194/acp-16-14463-2016

McDuffie, E. E., Smith, S. J., O'Rourke, P., Tibrewal, K., Venkataraman, C., Marais, E. A., Zheng, B., Crippa, M., Brauer, M., & Martin, R. V. (2020). A global anthropogenic emission inventory of atmospheric pollutants from sector- and fuel-specific sources (1970–2017): An application of the Community Emissions Data System (CEDS). *Earth System Science Data*, *12*(4), 3413–3442. https://doi.org/10.5194/essd-12-3413-2020

Miller, D. J., Actkinson, B., Padilla, L., Griffin, R. J., Moore, K., Lewis, P. G. T., Gardner-Frolick, R., Craft, E., Portier, C. J., Hamburg, S. P., & Alvarez, R. A. (2020). Characterizing Elevated Urban Air Pollutant Spatial Patterns with Mobile Monitoring in Houston, Texas. *Environmental Science & Technology*, *54*(4), 2133–2142. https://doi.org/10.1021/acs.est.9b05523

Murray, L. T. (2016). Lightning NOxand Impacts on Air Quality. *Current Pollution Reports*, *2*(2), 115–133. https://doi.org/10.1007/s40726-016-0031-7

NASA. (2023). *EOSDIS Worldview*. https://worldview.earthdata.nasa.gov/

NASA/LARC/SD/ASDC. (2022). *TRACER-AQ JSC G-V Aircraft Remotely Sensed GEOstationary Coastal and Air Pollution Events (GEO-CAPE) Airborne Simulator (GCAS) Data*. NASA Langley Atmospheric Science Data Center DAAC.

https://doi.org/10.5067/ASDC/SUBORBITAL/TRACERAQ/DATA001/GV/AircraftRemoteSensing/GCAS_1

Nowlan, C. R., Liu, X., Janz, S. J., Kowalewski, M. G., Chance, K., Follette-Cook, M. B., Fried, A., González Abad, G., Herman, J. R., Judd, L. M., Kwon, H.-A., Loughner, C. P., Pickering, K. E., Richter, D., Spinei, E., Walega, J., Weibring, P., & Weinheimer, A. J. (2018). Nitrogen dioxide and formaldehyde measurements from the GEOstationary Coastal and Air Pollution Events (GEO-CAPE) Airborne Simulator over Houston, Texas. *Atmospheric Measurement Techniques*, *11*(11), 5941–5964. https://doi.org/10.5194/amt-11-5941-2018

Palmer, P. I., Jacob, D. J., Chance, K., Martin, R. V., Spurr, R. J. D., Kurosu, T. P., Bey, I., Yantosca, R., Fiore, A., & Li, Q. (2001). Air mass factor formulation for spectroscopic measurements from satellites: Application to formaldehyde retrievals from the Global Ozone Monitoring Experiment. *Journal of Geophysical Research: Atmospheres*, *106*(D13), 14539–14550. https://doi.org/10.1029/2000JD900772

Ramboll. (2022a). Enhance MARINER Tool for Commercial Marine Emission Inventories Final Report. *Final Report*.

Ramboll. (2022b). *User's Guide COMPREHENSIVE AIR QUALITY MODEL WITH EXTENSIONS Version 7.20*. https://camx-wp.azurewebsites.net/Files/CAMxUsersGuide_v7.20.pdf

Riess, T. C. V. W., Boersma, K. F., Van Roy, W., de Laat, J., Dammers, E., & van Vliet, J. (2023). To new heights by flying low: Comparison of aircraft vertical NO_2 profiles to model simulations and implications for TROPOMI NO_2 retrievals. *Atmospheric Measurement Techniques*, *16*(21), 5287–5304. https://doi.org/10.5194/amt-16-5287-2023

Soleimanian, E., Wang, Y., Li, W., Liu, X., Griggs, T., Flynn, J., Walter, P. J., & Estes, M. J. (2023). Understanding ozone episodes during the TRACER-AQ campaign in Houston, Texas: The role of transport and ozone production sensitivity to precursors. *Science of The Total Environment*, *900*, 165881. https://doi.org/10.1016/j.scitotenv.2023.165881

TCEQ. (2021). *SIP Revision: Regional Haze*. Texas Commission on Environmental Quality. https://www.tceq.texas.gov/airquality/sip/bart/haze_sip.html

United States Census Bureau. (2022, June 13). *Metropolitan and Micropolitan Statistical Areas Population Totals: 2020-2022*. Census.Gov. https://www.census.gov/data/tables/time-series/demo/popest/2020s-total-metro-and-micro-statistical-areas.html

van Geffen, J., Eskes, H., Compernolle, S., Pinardi, G., Verhoelst, T., Lambert, J.-C., Sneep, M., ter Linden, M., Ludewig, A., Boersma, K. F., & Veefkind, J. P. (2022). Sentinel-5P TROPOMI NO_2 retrieval: Impact of version v2.2 improvements and comparisons with OMI and ground-based data. *Atmospheric Measurement Techniques*, *15*(7), 2037–2060. https://doi.org/10.5194/amt-15-2037-2022

van Geffen, J., Eskes, H. J., Compernolle, S., Pinardi, G., Verhoelst, T., & Lambert, J.-C. (2021). Sentinel-5P TROPOMI NO2 retrieval: Impact of version v2.2 improvements and comparisons with OMI and ground-based data. *Atmospheric Measurement Techniques*, *15*(7), 2037–2060. https://doi.org/10.5194/AMT-15-2037-2022

Verhoelst, T., Compernolle, S., Pinardi, G., Lambert, J.-C., Eskes, H. J., Eichmann, K.-U., Fjæraa, A. M., Granville, J., Niemeijer, S., Cede, A., Tiefengraber, M., Hendrick, F., Pazmiño, A., Bais, A., Bazureau, A., Boersma, K. F., Bognar, K., Dehn, A., Donner, S., … Zehner, C. (2021). Ground-based validation of the Copernicus Sentinel-5P TROPOMI NO₂ measurements with the NDACC ZSL-DOAS, MAX-DOAS and Pandonia global networks. *Atmospheric Measurement Techniques*, *14*(1), 481–510. https://doi.org/10.5194/amt-14-481-2021

Wagner, T., Warnach, S., Beirle, S., Bobrowski, N., Jost, A., Puķīte, J., & Theys, N. (2023). Investigation of three-dimensional radiative transfer effects for UV–Vis satellite and ground-based observations of volcanic plumes. *Atmospheric Measurement Techniques*, *16*(6), 1609–1662. https://doi.org/10.5194/amt-16-1609-2023

Weather Underground. (2023). *Houston, TX Weather History*. https://www.wunderground.com/history/daily/us/tx/houston/KHOU

Wiedinmyer, C., Akagi, S. K., Yokelson, R. J., Emmons, L. K., Al-Saadi, J. A., Orlando, J. J., & Soja, A. J. (2011). The Fire INventory from NCAR (FINN): A high resolution global model to estimate the emissions from open burning. *Geoscientific Model Development*, *4*(3), 625–641. https://doi.org/10.5194/gmd-4-625-2011

Page 10: [1] Deleted **Muhammad Omar Nawaz** **2/12/24 12:24:00 PM**

Page 10: [1] Deleted **Muhammad Omar Nawaz** **2/12/24 12:24:00 PM**

Page 10: [2] Change **Unknown**

Field Code Changed

Page 10: [2] Change **Unknown**

Field Code Changed

Page 10: [3] Deleted **Muhammad Omar Nawaz** **3/1/24 9:34:00 AM**

Page 10: [3] Deleted **Muhammad Omar Nawaz** **3/1/24 9:34:00 AM**

Page 10: [4] Change **Unknown**

Field Code Changed

Page 10: [4] Change **Unknown**

Field Code Changed

Page 10: [5] Deleted **Muhammad Omar Nawaz** **3/1/24 9:34:00 AM**

Page 10: [5] Deleted **Muhammad Omar Nawaz** **3/1/24 9:34:00 AM**

Page 10: [5] Deleted **Muhammad Omar Nawaz** **3/1/24 9:34:00 AM**

Page 10: [6] Formatted **Muhammad Omar Nawaz** **3/1/24 4:07:00 PM**

Font: Not Italic

Page 10: [6] Formatted **Muhammad Omar Nawaz** **3/1/24 4:07:00 PM**

Font: Not Italic

Page 10: [6] Formatted **Muhammad Omar Nawaz** **3/1/24 4:07:00 PM**

Font: Not Italic

Page 10: [6] Formatted **Muhammad Omar Nawaz** **3/1/24 4:07:00 PM**

Font: Not Italic

Page 10: [6] Formatted **Muhammad Omar Nawaz** **3/1/24 4:07:00 PM**

Font: Not Italic

Page 10: [6] Formatted **Muhammad Omar Nawaz** **3/1/24 4:07:00 PM**

Font: Not Italic

Page 10: [6] Formatted **Muhammad Omar Nawaz** **3/1/24 4:07:00 PM**

Font: Not Italic

Page 10: [7] Deleted **Muhammad Omar Nawaz** **3/1/24 9:34:00 AM**

Page 10: [7] Deleted **Muhammad Omar Nawaz** **3/1/24 9:34:00 AM**

Page 10: [7] Deleted **Muhammad Omar Nawaz** **3/1/24 9:34:00 AM**

Page 10: [8] Formatted **Muhammad Omar Nawaz** **3/1/24 4:07:00 PM**

Font: Not Italic

Page 10: [8] Formatted **Muhammad Omar Nawaz** **3/1/24 4:07:00 PM**

Font: Not Italic

Page 10: [9] Formatted **Muhammad Omar Nawaz** **3/1/24 4:07:00 PM**

Font: Not Italic

Page 10: [9] Formatted **Muhammad Omar Nawaz** **3/1/24 4:07:00 PM**

Font: Not Italic